RIGA TECHNICAL UNIVERSITY

Armands Šenfelds

RESEARCH AND DEVELOPMENT OF DC MICROGRIDS FOR ROBOTIC MANUFACTURING

Summary of the Doctoral Thesis

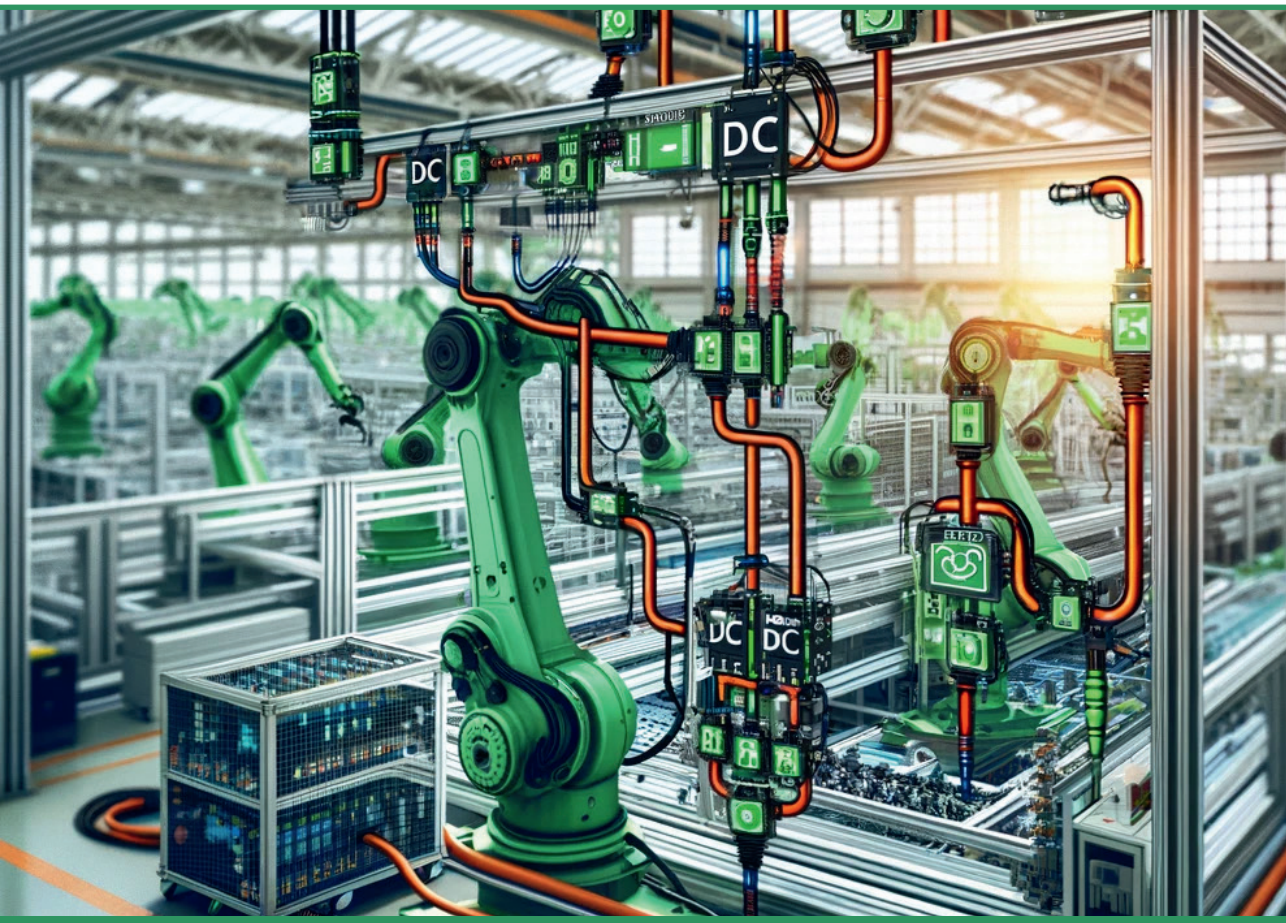

RTU Press
Riga 2023

RIGA TECHNICAL UNIVERSITY
Faculty of Electrical and Environmental Engineering
Institute of Industrial Electronics and Electrical Engineering

Armands Šenfelds
Doctoral Student of the Study Programme
"Computerised Control of Electrical Technologies"

RESEARCH AND DEVELOPMENT OF DC MICROGRIDS FOR ROBOTIC MANUFACTURING

Summary of the Doctoral Thesis

Scientific supervisor
Academician Professor Dr. habil. sc. ing
LEONĪDS RIBICKIS

RTU Press
Riga 2023

Šenfelds, A. Research and Development of DC Microgrids for Robotic Manufacturing. Summary of the Doctoral Thesis. Riga: RTU Press, 2023. 72 p.

Published in accordance with the decision of the Promotion Council "RTU P-14" of 4 October 2023, Minutes No. 04030-9.12.2/6.

The Thesis was supported by the European Social Fund within Project No. 8.2.2.0/20/I/008, "Strengthening of PhD students and academic personnel of Riga Technical University and BA School of Business and Finance in the strategic fields of specialization" of the Specific Objective 8.2.2 "To Strengthen Academic Staff of Higher Education Institutions in Strategic Specialization Areas" of the Operational Programme "Growth and Employment".

Cover picture generated by openAI DALL-E/ChatGPT 4.0.

https://doi.org/10.7250/9789934370199
ISBN 978-9934-37-019-9 (pdf)

DOCTORAL THESIS PROPOSED TO RIGA TECHNICAL UNIVERSITY FOR THE PROMOTION TO THE SCIENTIFIC DEGREE OF DOCTOR OF SCIENCE

To be granted the scientific degree of Doctor of Science (Ph. D.), the present Doctoral Thesis has been submitted for the defence at the open meeting of RTU Promotion Council on 29 December 2023 11.30 at the Faculty of Electrical and Environmental Engineering of Riga Technical University, 12/1 Āzenes Street, Room 212.

OFFICIAL REVIEWERS

Associate Professor Senior Researcher Dr. sc. ing. Jānis Zaķis
Riga Technical University

Prof. Dr. Ir. Rik W. De Doncker,
RWTH Aachen University, Germany

Senior Researcher PhD Toomas Vaimann
Tallinn University of Technology, Estonia

DECLARATION OF ACADEMIC INTEGRITY

I hereby declare that the Doctoral Thesis submitted for review to Riga Technical University for promotion to the scientific degree of Doctor of Science (Ph. D.) is my own. I confirm that this Doctoral Thesis has not been submitted to any other university for promotion to a scientific degree.

Armands Šenfelds ……. (signature)

Date: ……

The Doctoral Thesis has been prepared as a thematically united collection of scientific publications. It consists of a summary and 19 publications, and 1 patent. Publications have been written in English. The total number of publication pages is 202.

ACKNOWLEDGMENTS

I would like to express my deepest gratitude to my scientific supervisor, academician Professor Dr. habil. sc. ing. Leonīds Ribickis for his guidance, motivation and support in the scientific work.

I would also like to thank all employees of the RTU Institute of Industrial Electronics and Electrical Engineering, in particular Professor Ivars Raņķis, Professor Peteris Apse-Apsītis, Associate Professor Dāvis Meike for experience-based advice during the preparation of the Thesis, researchers Ansis Avotiņš, Mārcis Priedītis, Genadijs Zaļeskis for the support during the experimental research phase, my students Artūrs Paugurs and Oskars Bormanis, and researcher Kristaps Vītols for motivational discussions and excellent management of laboratory technical equipment.

During the research development phase, the time and support given by family and parents has been invaluable –, thank you very much!

CONTENTS

GENERAL OVERVIEW OF THE THESIS

Topicality of the research

Automated manufacturing developments are closely linked to the use of industrial robot equipment. According to research by the International Federation of Robotics (IFR), the annual number of newly installed robots globally reaches a historical high and exceeds half a million units. The total number of industrial robot machines worldwide in 2022 is estimated at 3,903,633 units, an annual increase of 12 %[1]. The total number of robots in Europe is estimated at 728,390 units, with a steady annual growth trend of 6 % [2]. Given that electricity is the primary energy source for modern and robotic production processes, the need for energy-efficient electricity supply solutions remains relevant. In the context of the possible transfer of production processes from Asia to the European region and higher electricity costs, initiatives to implement optimal energy technologies have a direct economic benefit. Public willingness and determination to change the structure of existing energy sources and move towards climate-neutral solutions also define new cooperation models and require a more flexible approach to developing electric energy management systems for production purposes. According to the road map defined by the European Commission Green Deal [3] to become a climate-neutral continent by 2050, programmes that contribute to changing energy systems in the production sector [4] have been created. Combinations of new renewable energy sources with energy storage, electromobility and efficient lighting and heating consumption promote the interest of engineers when considering combining or replacing existing AC infrastructure with DC electricity transmission technology [5]. The Thesis explores and demonstrates solutions for energy-efficient and flexible use of electrical energy in robotic production conditions by introducing DC electrical power transmission elements.

Main hypotheses and objectives

Hypotheses

1. Energy efficiency can be improved for industrial robot applications by utilizing electric energy recovery and reuse.
2. DC-type power supply solutions are suitable for implementing dynamic energy exchange processes.
3. DC microgrid is suitable for implementing energy-efficient robotic production systems.

Objectives

1. Analyse existing industrial robot technology as typical electric drive systems and explore new methods for practical energy recovery that are possible in realizing robotic manipulator motion tasks.
2. Explore improvements in the energy efficiency and functionality parameters of new robotic manufacturing plants using DC type power supply solutions and equipment.

In order to achieve the Thesis objectives, the following tasks were assigned:

- Analyse the operation of typical AC robot drive systems and define the characteristic parameters for controlling the process of dissipating braking energy.
- Development of modification solutions for existing robot drive system functionality for the energy recovery, storage and redistribution of braking energy in multi-robot systems.
- Develop examples of a local DC microgrid solution for the total power supply of a robotic manufacturing process in the form of laboratory equipment and mathematical computer models.
- Explore new operating modes and analyse the efficiency of key nodes on the DC microgrid.

Research tools and methods

Several methods have been used to analyse electrical systems and develop and test new solutions. Fluke, N4L power analyser, measurement equipment, and laboratory oscilloscopes have been used to obtain data characterizing electrical measurement and operating mode. The Data Translation universal DAQ platform is used to record data by adding appropriate auxiliary current and voltage measurement equipment.
Mathematical data processing and analysis have been performed using Matlab and Excel tools. Simulink, LTSpice, and PSpice tools have been used for the physical modelling of electrical circuits and systems. Printed circuit boards have been designed using Eagle and OrCAD software. Assembly of equipment and prototype design have been developed using SolidWorks and FreeCAD tools.
Laboratory setup and tailored power flow measurement equipment for time-synchronized data have been installed for conducting physical experiments, and controlled DC power flow and load test benches have been developed.

Scientific novelty

- Development of new interconnection circuit power electronic topologies for industrial robots and centralized storage systems.
- Development of a new solution for the physical replication of dynamic power profiles of electrical equipment in the DC microgrid at the laboratory scale.
- Developed and experimentally tested computer model of electrical drive systems and their interconnections for industrial robots.
- An equivalent computer model developed for the DC microgrid centralized AC/DC converter.
- A time-based analysis technique has been developed to obtain the required power and current parameters for cyclic processes to scale the electrical system and select equipment.

Practical novelties

The interconnection topology of industrial robots and centralized storage facilities and prototypes of equipment for the development of modular energy recovery systems have been developed and patented.
A detailed and time-synchronized data set of electrical energy flow measurements in an industrial DC microgrid with 13 measuring points has been obtained.
Analysis of DC microgrid power flows and determination of the amount and efficiency of recovered energy in an actual production process have been carried out.
New experimental testing facilities have been established to emulate the equivalent power profiles of different industrial consumers in real-time on the DC microgrid and study related effects.

Practical significance of the research

An experimental analysis has been carried out on a real DC microgrid, confirming the hypothesis of reuse of recovered energy.
A demonstration and experimental testing system of the DC microgrid at the laboratory level has been established.
In-depth knowledge of the introduction of DC microgrids for manufacturing purposes and the electrical design of industrial robot systems has been acquired throughout the research.

Structure and scope of the Thesis

The Thesis has been written in the form of a thematically unified set of scientific publications on the use of DC electrical systems and related elements to improve the performance of industrial robot installations. The Thesis has four chapters presenting the study of existing industrial robot electric drive systems, their modifications with DC interconnection elements, and the application of a full DC microgrid and a practical demonstration for robotic production.

Approbation of the Thesis

The summary of the Thesis comprises 19 publications and 1 patent. The results of the thesis work were presented in 12 conferences and 3 scientific journals.

1. Stupāns, A., Maksimkins, P., **Šenfelds, A.,** Ribickis, L. Industrial Robot Energy Consumption Analysis for Gravity-induced Opposing Force Minimization. In: *2022 7th IEEE International Energy Conference (ENERGYCON 2022*), Latvia, Riga, 9–12 May 2022. Piscataway: IEEE, 2022, pp.678-682. DOI 10.1109/ENERGYCON53164.2022.9830240
2. **Šenfelds, A**. Analysis of Motion Modelling Approaches for Industrial Robot Applications. In: *2019 IEEE 7th Workshop on Advances in Information, Electronic and Electrical Engineering (AIEEE 2019): Proceedings*, Latvia, Liepaja, 15–16

November 2019. Piscataway: IEEE, 2019, pp. 145–148. DOI 10.1109/AIEEE48629.2019.8977112

3. Apse-Apsitis, P., Vitols, K., Grinfogels, E., **Senfelds, A.,** Avotins, A. Electricity meter sensitivity and precision measurements and research on influencing factors for the meter measurements. In: *IEEE Electromagnetic Compatibility Magazine*, vol. 7, no. 2, pp. 48–52 DOI 10.1109/MEMC.2018.8410661
4. **Šenfelds, A**., Avotiņš, A., Apse-Apsītis, P., Grīnfogels, E., Ribickis, L. Investigation on Power Quality Parameters of Industrial 600V DC Microgrid Hardware. In: *2018 20th European Conference on Power Electronics and Applications (EPE'18 ECCE Europe): Proceedings*, Latvia, Riga, 17–21 September 2018. ISBN 978-907581528-3
5. **Šenfelds, A**., Apse-Apsītis, P., Avotiņš, A., Ribickis, L., Hauf, D. Industrial DC Microgrid Analysis with Synchronous Multipoint Power Measurement Solution. In: *2017 19th European Conference on Power Electronics and Applications (EPE '17 ECCE Europe): Proceedings*, Poland, Warsaw, 11–14 September 2017. Piscataway, NJ: IEEE, 2017, pp.3685-3690 DOI 10.23919/EPE17ECCEEurope.2017.8099322
6. Paugurs, A., **Šenfelds, A.**, Ribickis, L. Impact of Industrial Robot Tool Mass on Regenerative Energy. In: *Proceedings of 19th European Conference on Power Electronics and Applications, EPE'17 ECCE Europe*, Poland, Warsaw, 11–14 September 2017. Piscataway: IEEE, 2017, pp. 1–6. DOI 10.23919/EPE17ECCEEurope.2017.8099185
7. Grēbers, R., Gadaleta, M., Paugurs, A., **Šenfelds, A**., Avotiņš, A., Pellicciari, M. Analysis of the Energy Consumption of a Novel DC Power Supplied Industrial Robot. *Procedia Manufacturing*, 2017, Vol. 11, pp. 311–318. DOI 10.1016/j.promfg.2017.07.111
8. **Šenfelds, A**., Bormanis, O., Paugurs, A. Analytical Approach for Industrial Microgrid Infeed Peak Power Dimensioning. In: *2016 57th International Scientific Conference on Power and Electrical Engineering of Riga Technical University (RTUCON 2016): Proceedings*, Latvia, Riga, 13–14 October 2016. Piscataway, NJ: IEEE, 2016, pp. 328–331. DOI 10.1109/RTUCON.2016.7763140
9. **Šenfelds, A.**, Bormanis, O., Paugurs, A. Modelling of AC/DC Power Supply Unit for DC Microgrid. In: *Advances in Information, Electronic and Electrical Engineering (AIEEE 2015):Proceedings of the 2015 IEEE 3rd Workshop*, Latvia, Riga, 13–14 November 2015. Piscataway: IEEE, 2015, pp. 81–84. DOI 10.1109/AIEEE.2015.7367294
10. **Šenfelds, A.** Analysis of Cyclic DC Load Currents for Intelligent Electrical Protection. In: *2015 56th International Scientific Conference on Power and Electrical Engineering of Riga Technical University (RTUCON):Proceedings*, Latvia, Riga, 14–14 October 2015. Riga: Riga Technical University, 2015, pp. 165–168. DOI 10.1109/RTUCON.2015.7343162
11. Paugurs, A., **Šenfelds, A**. Design of a Motor Drive System for Bidirectional DC Power Flow Control. In: *2015 56th International Scientific Conference on Power and Electrical Engineering of Riga Technical University (RTUCON*), Latvia, Riga, 14–14 October 2015. Riga: 2015, pp. 265–268. DOI 10.1109/RTUCON.2015.7343145
12. **Šenfelds, A**., Vorobjovs, M., Meike, D., Bormanis, O. Power Smoothing Approach within Industrial DC Microgrid with Supercapacitor Storage for Robotic Manufacturing Application. In: *2015 IEEE International Conference on Automation*

Science and Engineering (CASE 2015): Automation for a Sustainable Future: Proceedings, Sweden, Gothenburg, 24–28 August 2015. Piscataway: IEEE, 2015, pp. 1333–1338. DOI 10.1109/CoASE.2015.7294283

13. Apse-Apsītis, P., **Šenfelds, A.**, Avotiņš, A., Paugurs, A., Priedītis, M. Power Measurement and Data Logger with High-Resolution for Industrial DC-Grid Application. In: *Power Electronics and Applications (EPE'17 ECCE Europe), 2017 19th European Conference*, 2015, Vol. 9, pp. 36–42. DOI 10.1515/ecce-2015-0010
14. **Šenfelds, A.**, Paugurs, A. Electrical Drive DC Link Power Flow Control with Adaptive Approach. In: *2014 55th International Scientific Conference on Power and Electrical Engineering of Riga Technical University (RTUCON): Proceedings*, Latvia, Riga, 14–14 October 2014. Riga: RTU Press, 2014, pp. 30–33. DOI 10.1109/RTUCON.2014.6998195
15. Meike, D., **Šenfelds, A.**, Ribickis, L. Power Converter for DC Bus Sharing to Increase the Energy Efficiency in Drive Systems. In: *IECON 2013 – 39th Annual Conference of the IEEE Industrial Electronics Society: Proceedings*, Austria, Vienna, 10–13 November 2013. Piscataway, NJ: IEEE, 2013, pp. 7197–7202. DOI 10.1109/IECON.2013.6700329
16. Priedītis, M., Meike, D., **Šenfelds, A.** Micro Controller Unit Process Time Sharing and Digital Filter Analysis in Industrial Energy Exchange System. Power and Electrical Engineering. Vol. 31, 2013, pp. 106–111. ISSN 14077345
17. **Šenfelds, A.**, Meike, D. Industrial Shared DC Bus Application: Common Ground Current Observation. In: *54th International Scientific Conference of Riga Technical University. Section of Power and Electrical Engineering: Digest Book and Electronic Proceedings*, Latvia, Riga, 14–14 October 2013. Riga: RTU Press, 2013, pp. 11–13. ISBN 978-9934-10-470-1
18. **Šenfelds, A.**, Raņķis, I. Common Node Circular Current Examination in Shared DC Bus Power System. In: *13th International Symposium "Topical Problems in the Field of Electrical and Power Engineering. Doctoral School of Energy and Geotechnology II"*, Estonia, Pärnu, 14–19 January 2013. Pärnu: Elektriajam, 2013, pp. 85–88. ISBN 978-9985-69-054-3
19. Raņķis, I., Meike, D., **Šenfelds, A.** Utilization of Regeneration Energy in Industrial Robots System. *Enerģētika un elektrotehnika*. No. 31, 2013, pp. 95–100. ISSN 14077345
20. Lebrecht, M., Meike, D., Rankis, I., **Senfelds, A.** Produktionsanordnung mit wenigstens zweiAntriebssystemen. German Patent DE 10 2013 010 462 A1, Patent publication date: 27.03.2014

INTRODUCTION

Without highly automated technological solutions, a state-of-the-art manufacturing process that creates high-added value physical products of many units is hard to imagine. Industrial robot equipment is often used in processes characterized by product type repeatability, precise assembly conditions, hazards to humans and harmful conditions. An industrial robot is a complex machine that provides a computer-controlled process through an electromechanical system. It often uses electrical energy for its operations and fits into the broader production organization and necessary material and energy supply system. Developments related to the impact of geopolitical processes and significant increases in energy prices have contributed to the need for a new approach, diversifying energy sources, promoting system flexibility and efficient end use of energy, for which incentives are being developed [6]. Given the extensive process of introducing new technologies from an experimental prototype to fully defined everyday applications and the application of related standards and regulations, several focus groups and associations of engineers have emerged, as well as research projects AREUS [7] and DC Industrie [8], to promote the practical implementation of DC systems.

Given that DC systems can benefit from a wide range of applications from large-scale power generation and transmission, such as offshore wind farms and HVDC high-voltage direct current transmission lines, to, for example, a single power supply standard for domestic appliances, USB-C[9], organizations have developed with an intent to explore targeted applications. The Current OS Foundation [10] and DC systems [11] want to promote high-end, low-voltage DC applications and implement the relevant system management and coordination standards. The research organization FEN – Flexible Electrical Networks [12] – is promoting the deployment of DC system applications for the application of distribution and transmission networks to deploy future flexible energy systems. The activities and applications carried out in the Thesis are related to a large extent to the scope of the recently established ODCA – Open DC Alliance – for the exploration of industrial DC products and solutions. Given that DC industrial networks are entering the development phase as long-term investment projects for practical applications [13],[14], economic rationale and industry interest are also predictable in the coming years. The knowledge and experience gained in developing the Thesis are also helpful in developing local SME-scale DC systems, considering the need to achieve renewable energy and efficient energy use targets under the National Climate and Energy Plan 2030[15].

1. ANALYSIS OF TYPICAL ELECTRIC DRIVE SYSTEMS FOR AC INDUSTRIAL ROBOTS

In this chapter, the main properties of industrial robot kinematic systems, motion execution and electrical drive systems are discussed. The author's publications 1 an 2 are related to Chapter 1. For an overview of the intrinsic characteristics and functionality of an industrial robot installation linked to the subsequent analysis of electric drive systems, it is beneficial to examine the classification of robotic equipment. The methodology proposed by the International Robotics Association is considered a comprehensive method for classifying robotic equipment, including manufacturing applications [16]. According to the selected classification procedure, a distinction can be made between several types of equipment eligible as robotic equipment for production purposes. Firstly, it is possible to divide the installations according to their location – stationary and mobile.

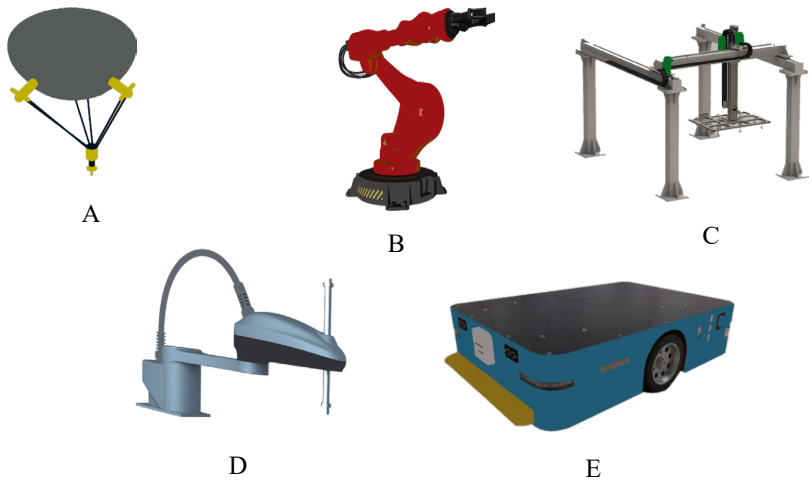

Fig. 1.1. Industrial robot types: A) – Delta; B) – articulated manipulator; C) – Cartesian (linear); D) – SCARA-type; D) – autonomous guided vehicle (AGV).

- The Delta (parallel) robot comprises a base platform incorporating an electric drive and work platforms with a work tool driven by three levers. The specific feature of such a structure is the possibility of reducing the moving parts' weight and obtaining rapid accelerations and precision for the work platform. Typical application directions are packaging, precise assembly and material handling. The market-available mass-produced robot equipment payload is up to 15 kg [16].
- An articulated robot is a machine that consists of at least three rotating joints, and the kinematic system has vast flexibility capabilities that would be somewhat comparable to the range of motion of the human arm from the shoulder onwards. The advantages of such a system are excellent reachability and workspace compared to the robot's size. An articulated robot has been widely used as a typical manipulator in highly automated

manufacturing processes such as automotive, metalworking and electrical equipment manufacturing.

- The Cartesian (linear) robot workspace is a rectangular area in a space that can be described by the coordinates X, Y, and Z adopted in the Cartesian coordinate system, placed perpendicular to each other. Robotic manipulators of this type are widely used in various types of CNC processing machines, lifting and material handling tasks. The device's design allows for relatively simple movement control, but limitations include the inability to reach the working space under the objects.
- The SCARA-type robotic manipulators are comparable to the human arm's operating principle but with more limited movement flexibility, mainly using the ability to bend the arm in the elbow part. The vertical movement of the end effector is carried out only with the last drive built into the manipulator structure, and positioning in a horizontal plane is done with two parallel rotating axes. The drawback of this manipulator is also the ability to perform operations from the top, but the machine is widely used in automated assembly processes, especially in electronics.
- Autonomous guided vehicles (AGV) are also regarded as robotic devices, the control of which can be carried out employing built-in elements (cameras, sensors) and objects integrated into the environment (magnetic strips, dots, signal wires). The AGVs are widely used in automated manufacturing with the introduction of typical packaging elements in the materials supply. As new concepts of flexible production organization evolve, mobile platforms are also seen as a base for installing other production equipment in a customizable environment.

The Thesis provides a focused view of the most popular industrial robot manipulators based on the principle of kinematic structure of the articulated serial manipulator applied in industrial manufacturing. Examples of typical applications are those for ancillary assembly and production tasks in which the robot serves as a platform for installing tools with a significant weight exceeding 100 kilograms.

The role and dynamics of electric drive

The role of electric drive in an industrial robot is to realize time-related positioning demand for individual robot axes. Incremental command of rotational position of each axis is defined following the planned trajectory of the robot end tool, which includes simultaneous calculation of positioning of all axes. It is realized with the help of a robot controller. Figure 1.2 shows a typical industrial robot manipulator and its schematic structure. In this case, the machine is designed as a combination of a series of six rotary joints, with the symbols A1 to A6 indicating the position of the rotary axes.

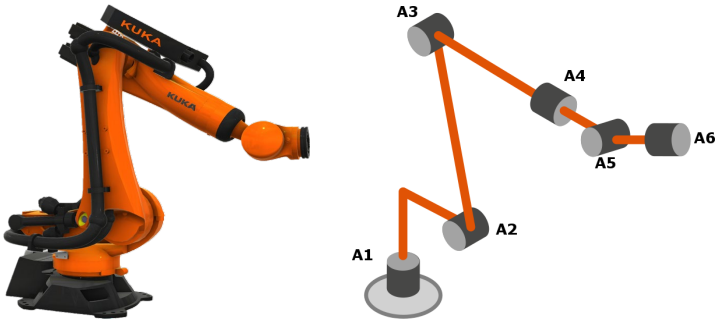

Fig. 1.2. The structure of articulated 6-axis industrial robot manipulator.

An appropriate kinematic model can describe an industrial robot manipulator as a system of series interconnected solid bodies, including moving joint elements [17]. This way, it is possible to analytically investigate possible variations in the positions of individual joints and also the areas or working space available for the end tool of the manipulator.

However, techniques based on applying an appropriate dynamic model are used. Like in the kinematic approach, it is possible to distinguish the direct and inverse dynamics model for the particular robotic manipulator configuration-related dynamics process. The relationship between the individual axis torques of an industrial manipulator and the changes in the positions of the robot manipulator can be described using an inverse dynamics calculation.

Function (1.1) determines the instantaneous values of the required individual axle torque set τ for individual drive nodes to execute the manipulator motion.

$$\tau = f(q, \dot{q}, \ddot{q}, f_{ext}) \tag{1.1}$$

The described manipulator motion is expressed as a system of the set of individual axles of angular positions q, velocities $\dot{q}$, and angular accelerations of $\ddot{q}$. The force component of the external action produced by the robot manipulator is described on each of the axes by a set f_{ext}. As this function describes the dependence of the system input value, which is the torque produced by the drive, on the output parameter set of the manipulator system, this approach is referred to as *the inverse dynamics model*.

The operation of the actual system is described by a *direct dynamic model* (Eq. (1.2)), where the acceleration of each axis $\ddot{q}$ depends on the axis torques τ, angular position q, rotational speed $\dot{q}$ and interaction of external forces f_{ext}.

$$\ddot{q} = f(\tau, q, \dot{q}, f_{ext}) \tag{1.2}$$

For detailed analysis of the inverse dynamics process of the series kinematics-based robot manipulator (Eq. (1.1)), it is described in an expanded form according to Eq. (1.3).

$$\tau = D(q)\ddot{q} + C(q, \dot{q})\dot{q} + f(\dot{q}) + g(q) + e(q) \tag{1.3}$$

Axis torques τ are obtained by the combination of the following effects on the axes of the robot:

$D(q)$ – a matrix, the elements of which depend on the location of current robot axes and the mass of individual parts of the robot describing the induced inertia effect;

$C(q, \dot{q})$ – a matrix with elements describing Coriolis and centrifugal forces;

$f(\dot{q})$ – the vector describing friction events;

$g(q)$ – the vector describing the moments produced by gravity projections on the axes;
$e(q)$ – the vector describing projections of external force action moments on axes.
The main objective of an industrial robot is based on the execution of a real-time continuous work tool positioning task that is translated to position commands of individual axis drives and executed synchronized. Given the need for precise motion, the drive units of industrial robots are most often implemented by electric drives and precision gear drives. Hydraulic and pneumatically controlled joints have also been popular in the early stages of the development of industrial manipulators. Given the trends and affordability of electrical drive technologies from a cost and functionality perspective, electrical drives have become the leading positioning solution in robot technology.

Overview of an architecture of industrial robot controller

According to the robot configuration mentioned earlier, the robot controller structure is designed to provide a synchronized operation of 6-axis drives. Figure 1.3 shows the inner build of the KUKA KRC4 industrial robot controller. From an electrical drive analysis point of view, it is essential to identify three functional units – an AC rectifier that provides DC voltage for two combined inverter units. Inverters provide control of PMSM servo drives grouped by axis mechanical load: 1–3 axes and 4–6 axes, respectively.

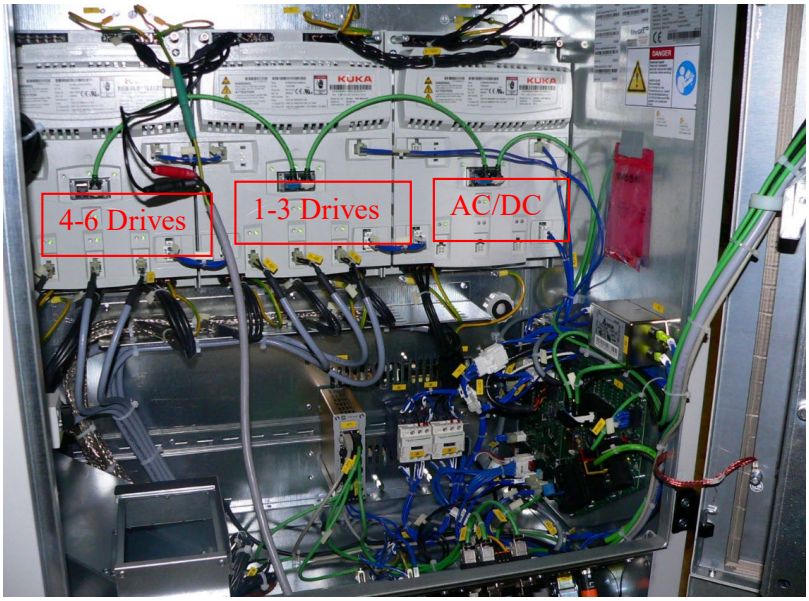

Fig. 1.3. Arrangement of KUKA KRC4 robot controller electrical drives.

Robot manufacturer KUKA provides a robot controller as a modular system and applies manufacturer-specific electrical functional unit designations KPP – KUKA power Pack, and KSP – KUKA Servo pack. For experimental activities related to the Thesis, an industrial robot

with a 210 kg payload capacity was applied, and an AC-type KRC4 controller with the following KPP and KSP parameters was configured according Table 1.1.

Table 1.1

Nominal Data of ElectricalDrive Elements of the KUKA KRC4 Robot Controller

Device	Input parameters	Output parameters
KPP 600-20	3PE AC 400/480 V 20 A 50/60 Hz 14/17 kW	2 PE DC 565/675 V 25 A 14/17 kW
KSP 600-3X40	2 PE DC 565/675 V 25 A	3 PE AC 0-400/480 V 17 A 0–500 Hz 12/14 kW
KSP 600-3X20	2 PE DC 565/675 V 25 A	3 PE AC 0–400/480 V 9 A 0–500 Hz 6/7 kW
Servo drives 1–3	Uph 201 V, Iph 9.5 A	Nn/Nmax 3000/5000 rpm, 4.9 kW
Servo drives 4–6	Uph 152 V, Iph 5.6 A	Nn/Nmax 3000/7200 rpm, 2.3 kW

The figure shows an extended structural diagram of the KRC4 controller, which distinguishes between 24 V voltage level equipment and the equipment connected to the DC bus, presented on a grey background colour.

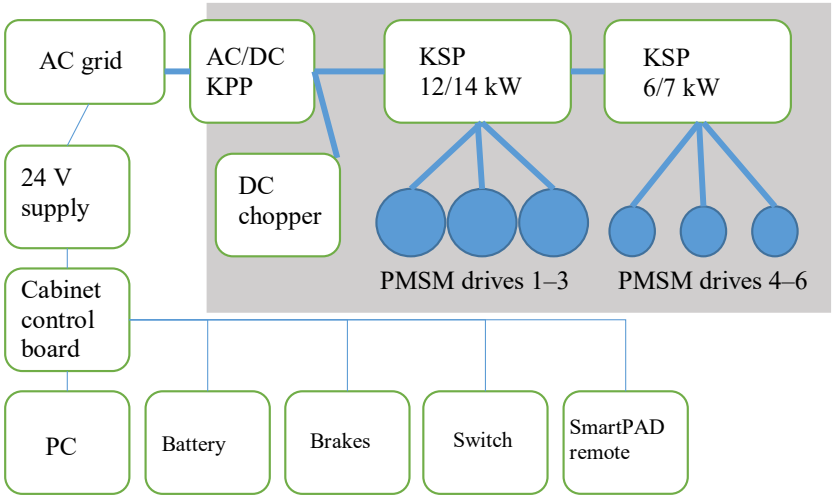

Fig. 1.4. Structure diagram and electric power supply of the KUKA KRC4 controller.

Power consumption or electrical drive recuperation depends on the robot's planned motion program performance [20]. In practice, such data on the power consumed by individual electrical machines or a group of electrical drives during the execution of the program can be obtained by several methods.

- A detailed robot modelling approach, as described in [18] and [19], predict a sequential calculation of the energy flows of an industrial robot, taking into account the power of

individual electrical machines and friction losses. This approach makes it possible to achieve a universal model that is also suitable to address the challenges of motion optimization taking into account energy consumption.

- Practical measurements by connecting current and voltage measurements to the DC bus allow recording of the data obtained, which, employing subsequent processing combined with the measurement of the power consumed by individual inverters, enable a sum of power of the DC bus. Figure 1.5 represents the resulting change in total DC bus power due to a practical measurement of 2 robots.

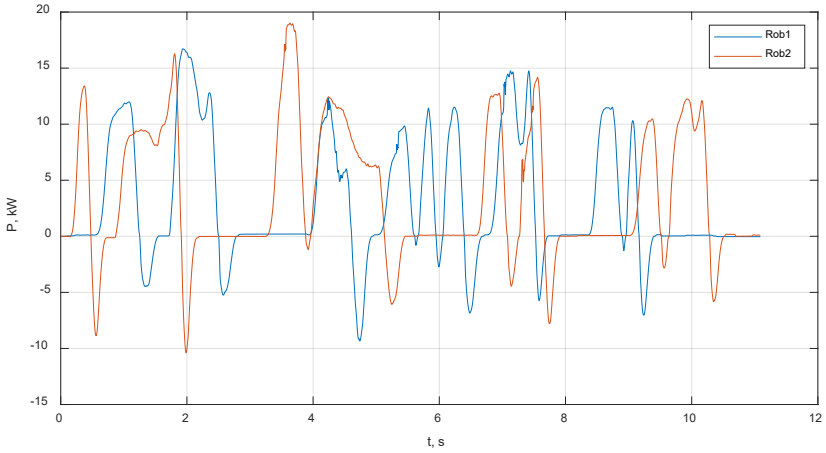

Fig. 1.5. Experimentally obtained DC bus power profiles in two industrial robot operations.

- Alternatively, the recording function of the internal parameters of the robot controller is also mentioned as a method to obtain individual axis power consumption or associated values, such as current and voltage data. This is possible through, e.g., KUKA Trace software feature, which is primarily designed for diagnostics of the robot's internal processes, but the data generated during movement can also be used for further modelling or optimization tasks (Eqs. (1) and (2).

If data are available on the dynamic electric power profile of the 6-axis drive of an industrial robot, an equivalent model of the electrical system can be developed to study the operation of the electric drive and the DC bus. The structure of the model is shown in Fig. 1.6.

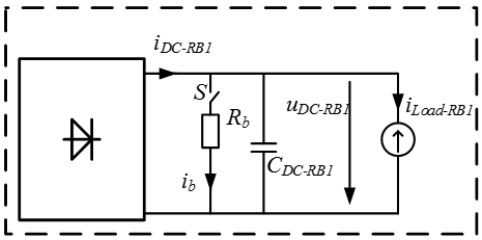

Fig. 1.6. A model of electric system of industrial robot manipulator for AC power supply.

The primary energy source is the AC grid, which is supplied to the DC bus via an uncontrolled rectifier. The value of the rectified voltage at idle operation of the rectifier depends on the grid voltage according to Eq. (1.4), where U_{L-L} is the voltage between the phases in the three-phase system and U_{DCidle} is the value of the rectified voltage at no load.

$$U_{DCidle} = \sqrt{2}U_{L-L} \tag{1.4}$$

Thus, it can be concluded that at the 400 V voltage system standard in Europe, the voltage of the DC stage is 565 V at no load.

Practical analysis of the KRC4 robot controller has made it possible to determine the total combined DC bus capacitance. The value of C_{DC-RB} is 1.3 mF. Similarly, the braking resistor value, R_B , has been determined – 11 Ω. The application of the braking resistor follows from the principle of hysteresis-type control, which measuring the voltage of the DC bus U_{DC} compares to 2 voltage levels U_{RbON} – 685 V and U_{RbOFF} – 665 V. At 685 V DC bus voltage, the energy dissipation within the resistor is initiated until a reduction to 665 V is achieved, and the braking resistor is switched off.

The dynamic power profile of an industrial robot $P_{Load}(t)$ is realized by modelling the equivalent power source according to the equation:

$$I_{Load}(t) = P_{Load}(t)/U_{DC}(t) \tag{1.5}$$

Figure 1.7 shows the implementation of the model structure in the Matlab Simulink modelling environment.

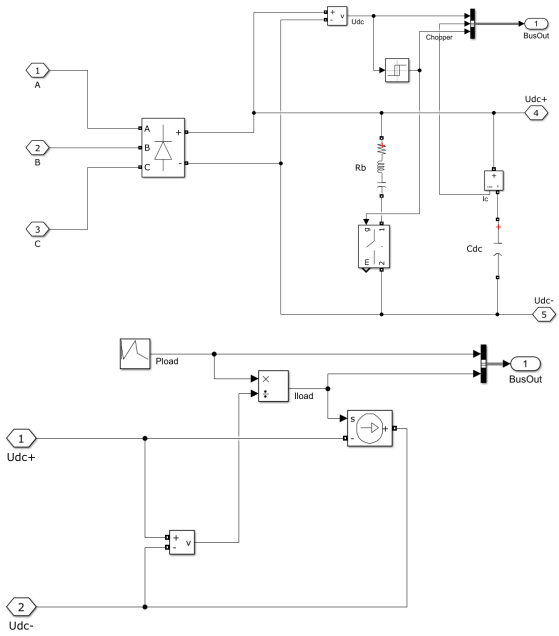

Fig. 1.7. Implementation of AC industrial robot electric model in Matlab/Simulink: rectifier, filter capacitor and brake resistor circuit (above), and equivalent dynamic axis load element (below).

Simulation of the experimentally obtained load profile with the model described above results in the DC voltage variations and braking resistor operation Fig. 1.8.

The established model is valuable for further research on energy efficiency improvement measures. The following chapter explicitly considers modifications to existing AC industrial robot drives by introducing DC network elements.

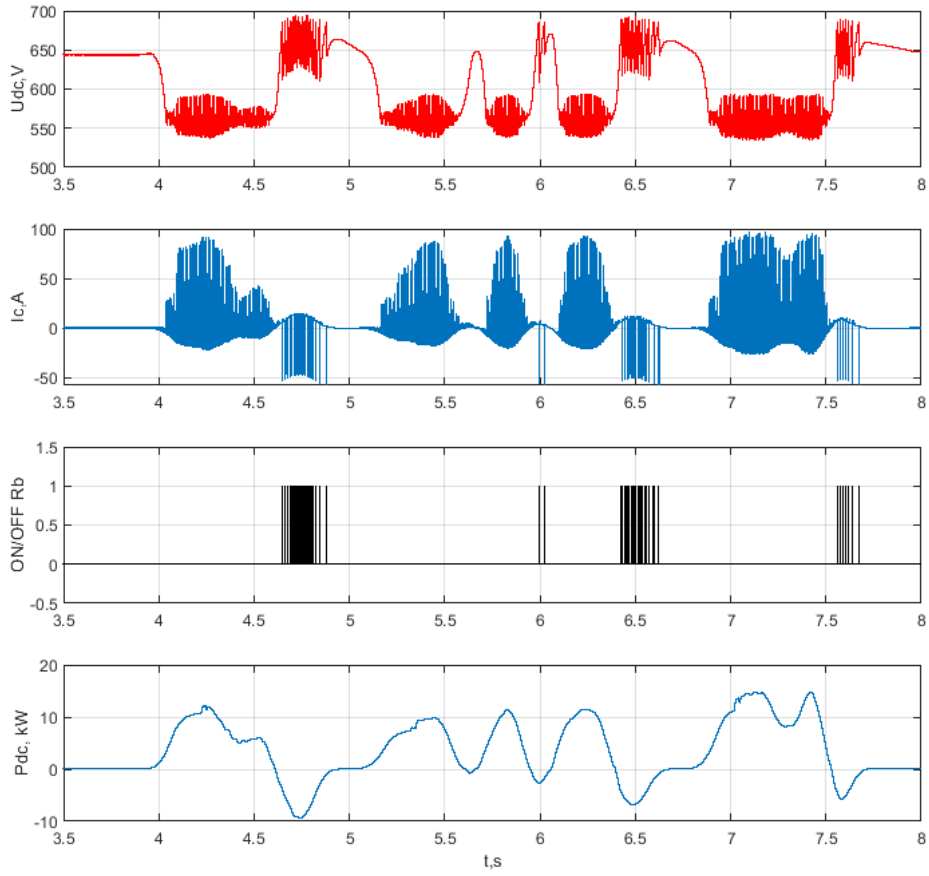

Fig. 1.8. Results of the equivalent electric model of an industrial robot: U_{DC} – DC bus voltage variation; I_C – DC bus capacitor current, braking resistor operating command, and the executed industrial robot program power profile P_{DC}.

2. DEVELOPMENT OF DC-BASED CONVERTERS FOR ENERGY-EFFICIENT MODIFICATION OF AC INDUSTRIAL ROBOTS WITH TRADITIONAL FREQUENCY CONVERTERS

This chapter presents an approach for energy efficiency improvement by modifications of a typical AC electrical supply-based industrial robot. The author's Publications 15–20 represent the findings of this chapter.

By analytical observation of the design of typical AC robot controllers, it can be concluded that braking motions are present depending on the performance of the trajectory execution task. During such motions, recuperated energy is accumulated in the DC capacitor and by the presence of a predefined higher voltage level is dissipated by the braking resistor. Thus, there is a direct potential for improving energy efficiency if the share of dissipated energy in normal working conditions is reduced. Several possible ways of improving energy efficiency from the point of view of optimization of the electrical system are summarized below, but there are also other methods related to optimizing motion trajectories, and software is known [21].

Each of the presented options is increasingly relevant for using DC power transmission in robotic systems:

- Controlled bidirectional rectifier application.

Simply replacing an uncontrolled rectifier with a bidirectional rectifier is significantly more expensive than inserting additional capacitance into the DC bus. Considering related requirements for AC grid power quality and the relatively low individual load power per converter, such a solution should be considered in the context of a significant DC side electrical system dimension and connected load pool.

- Increasing the capacitance of the DC bus.

Such an option requires additional capacitors in each robot controller, which entails additional costs [22] but also has potentially positive aspects in terms of increased system reliability [23]. The optimal choice of capacitor capacity depends on the most significant recovery energy peak generated during the motion trajectory execution task performed. This solution is considered appropriate in cases where there are one or few robot controllers distributed over longer distances in the manufacturing area.

- Interconnection of DC bus of multiple industrial robots.

An alternative approach is the introduction of additional capacitance and its availability through the connection of multiple robots to a shared capacitor module for the efficient use of braking energy. This approach is analysed and discussed in detail along with practical implementation in the following chapter.

- Provision of DC power supply.

As a large-scale solution involving the use of robots and the bidirectional energy exchange potential of industrial drives a single DC microgrid is created with one centralized AC connection.

Interconnection of DC bus of multiple industrial robots

For the short-term accumulation and reuse of braking energy, the capacitance of the DC bus may be utilized if the operating principles of the installation allow for variation in individual DC bus voltage U_{DC_i}. Figure 2.1 depicts the principle for connecting the DC bus of individual drives with a common capacitor module *C*.

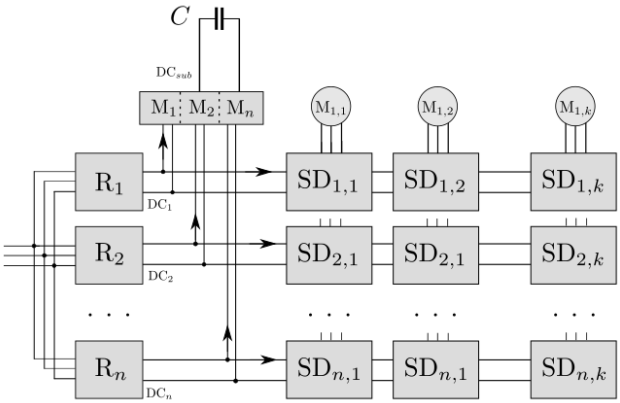

Fig. 2.1. Interconnection of multiple electrical drive inverter *SD* groups with input rectifiers, *R,* with shared DC bus and additional capacitance, *C*, application (the autor's Publication 15).

Each drive system shall retain the existing input rectifier and the structure of the DC bus. Additionally, the interconnection module *M* is introduced, allowing the power flow to be controlled between individual robots and a common capacitor *C* and respective voltage U_C.

Key operating principles for interconnection modules:

- storage and efficient use of recovered energy;
- do not affect the regular operation of the existing drive system configuration providing power from the AC grid.

Within the framework of the Thesis, several versions of the interconnection circuit have been established, which can be divided into asymmetric commutation interconnection (1 version) and symmetric commutation interconnection circuit (2 versions) topology solutions.

Asymmetric interconnection circuit analysis

In order to have practical implementation, an electrical circuit diagram was set up as illustrated in Fig. 2.2.

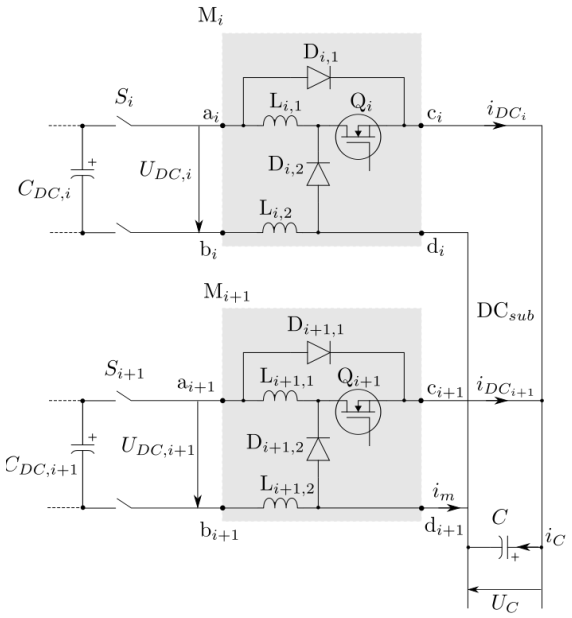

Fig. 2.2. Asymmetric commutation DC interconnection circuit.

In order to ensure the exchange of recovered energy through the external capacitor module, the hysteresis-type control principle is applied, and the capacitor voltage control parameters U_{ON} and U_{OFF} are introduced. The flow of recovered energy to central capacitor *C* occurs by natural commutation and diode *D*. The energy flow and reuse of pre-accumulated energy in each of the robot drives takes place by operating the *Q* semiconductor switch, which is commutated by the following principle (Eq. (2.1)):

$$Q \text{ state} = \begin{Bmatrix} ON \; if \; U_C > U_{ON} \\ OFF \; if \; U_C \leq U_{OFF} \\ previous \; state \text{ otherwise} \end{Bmatrix}. \tag{2.1}$$

The module interconnection instance voltage trigger level U_{ON} of the hysteresis control is higher than the disconnection instance level U_{OFF}, which allows for a more stable operation by introducing a deadband between these values.

$$U_{ON} \geq U_{OFF} \tag{2.2}$$

Practical testing of the presented circuit was carried out (the author's Publication 19) with the interconnection of two industrial robots, resulting in terms of energy consumed over a 1-hour working period Table 2.1.

Table 2.1

Energy Consumption Results for the Asymmetrical Connection of Two Industrial Robots

Robot application	Welding	Handling
Without DC interconnection, kWh	3.66	6.44
With DC interconnection, kWh	3.45	5.11
Difference, %	–5.6	–20.5

Experimentally measured voltage variation and corresponding current during operation are presented in Fig. 2.3.

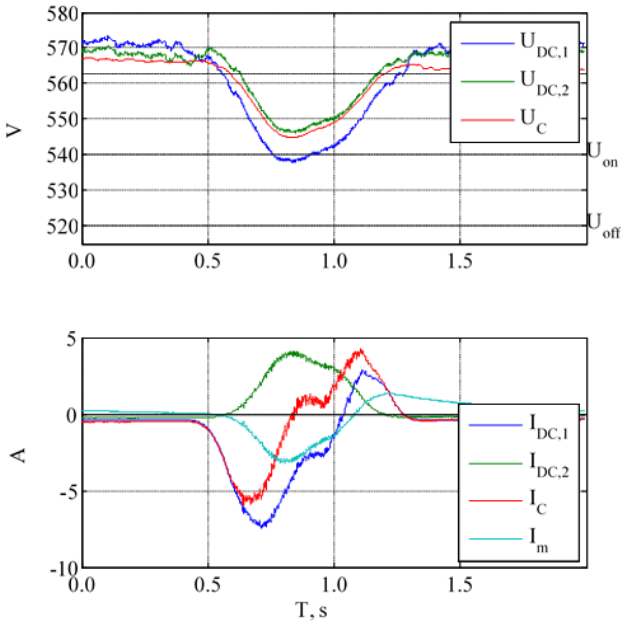

Fig. 2.3. Asymmetric interconnection operating mode at control voltage parameters U_{ON} = 540 V and U_{OFF} = 520 V.

During the experimental test, an *Im* current flow has been observed due to potential equalization effects imposed by directly coupled negative DC bus poles (the author's Publications 17 and 18).

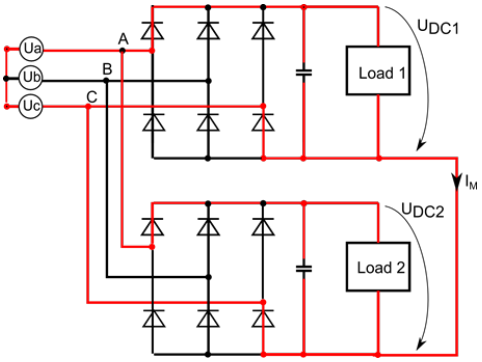

Fig. 2.4. Equalizing current circuit in the case of asymmetric connection.

Such an effect creates a new operation mode for the load of rectifiers. Due to the possibility of modifying existing equipment and developing potential diagnostic errors, it was decided to consider the introduction of symmetric switching modules for future work. It is also important to ensure that discharge of the main capacitor Uc is interrupted at the voltage U_{OFF} before the no-load output voltage U_{DCidle} of the rectifier is reached at 565 V when the 230 V phase voltage system is used.

$$U_{OFF} \geq U_{DCidle} \tag{2.3}$$

The work on creating a new type of interconnection circuit for the task under examination was continued.

Development of symmetric interconnection circuit

Based on the necessary modifications and previous test experience, a new type of DC link interconnection topology (the author's Publication 20) was developed and patented to ensure synchronous switching of both DC circuit poles in the event of interconnection.

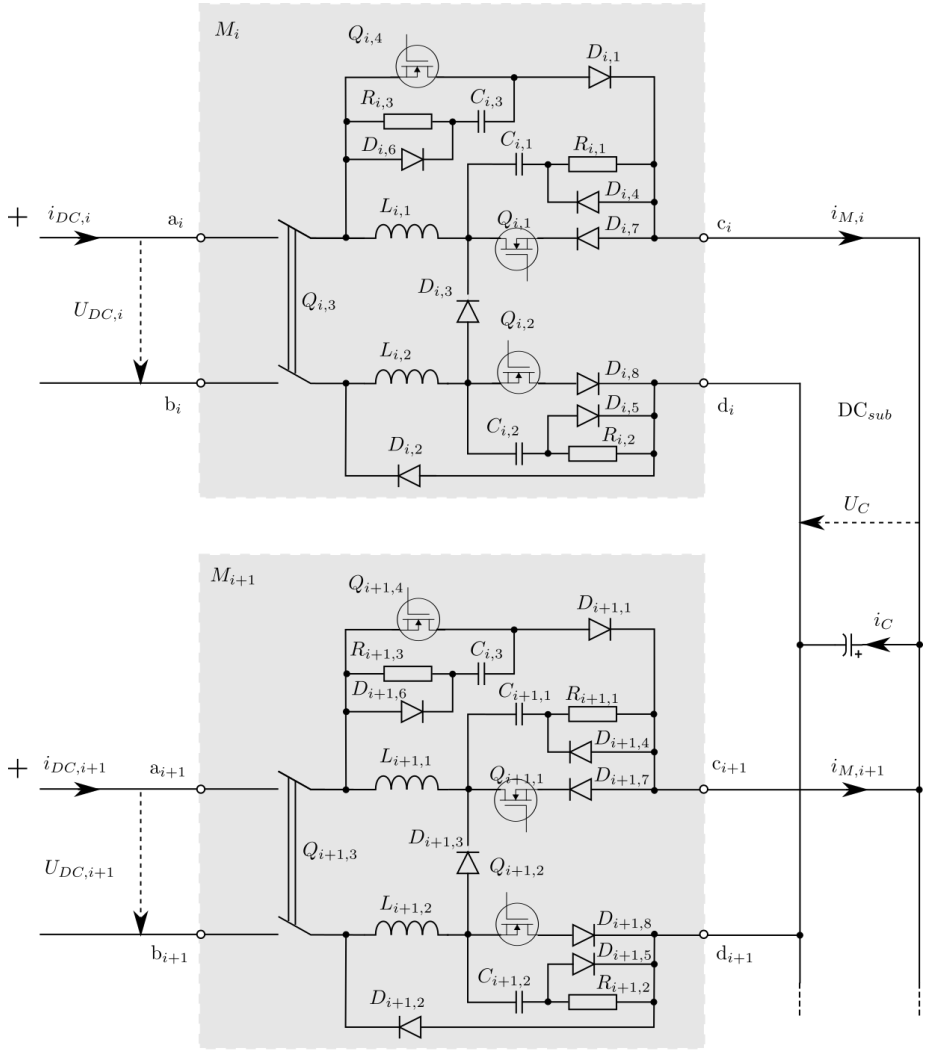

Fig. 2.5. Symmetric commutation DC interconnection circuit.

The main differences are the introduction of an additional semiconductor switch for switching the other pole and the possibility of conducting a controlled pre-charge of the main capacitor from one of the connected DC buses of industrial robots. The interconnection prototype circuit power device module without peripherals is shown in Fig. 2.6.

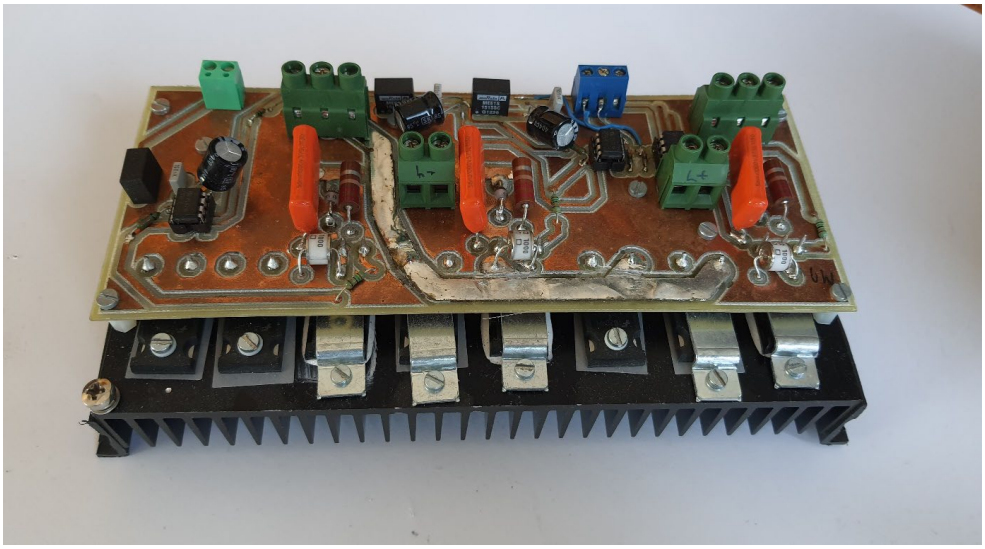

Fig. 2.6. Prototype of symmetric interconnection circuit power switch board.

The installation was subsequently assembled and experimentally tested under industrial conditions in collaboration with Mercedes Benz AG (former Daimler AG), Germany, using industrial robot manipulators KUKA KR210 with additional weight elements 150 kg and 200 kg as reproduced Fig. 2.7.

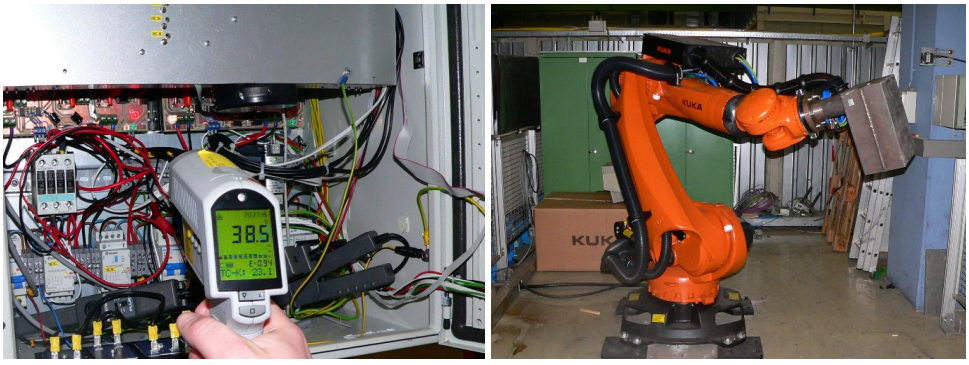

Fig. 2.7. Experimental verification in production area: interconnection module with peripheral devices (left) and one of the interconnected KUKA KR210 industrial robots (right).

During the test, electrical parameter data recording and energy consumption estimation were performed with the equipment shown in Fig. 2.7, FLUKE AC power analyser, and the data logging system.

Fig. 2.8. Application of DC interconnection electric parameter data recording and AC power analyser devices.

A 20-minute operation period analysis was carried out on the power consumed for a 2-industrial robot interconnected system, and the obtained results are presented in Table 2.2.

Table 2.2

Average Power Consumed in the Case of a 2-robot System

Robot application	**Handling – 20 min (no extra weight)**	**Handling – 20 min (with additional weights of 150 and 200 kg)**
Average power without DC interconnection, kW	6.23	8.67
Average power with DC interconnection, kW	4.92	5.11
Difference, %	–21.1	–22.7

The pilot test demonstrates the positive impact of the preferred option on increasing energy efficiency for this robotic application, reaching savings of up to 22.7 % in average energy consumption. It is important to note that, under actual production conditions, the operational tasks of individual robots may vary considerably according to the required motion dynamics, and relatively fast motion and strong recovery modes movement profiles were used in this test to test electrical parameters for the prototype created.

Due to the actual performance of the system, the direct voltage measurements of both individual robots and the shared DC bus, it was possible to develop an equivalent computer model using the modelling tools of Matlab and Simulink, as well as to compare the performance of the model

and the actual measured system (the author's Publication 15). Figure 2.9 compares the results of dynamic variation of the most characteristic parameters in a similar operating mode with the same U_{ON} = 600 V and U_{OFF} = 580 V control parameters.

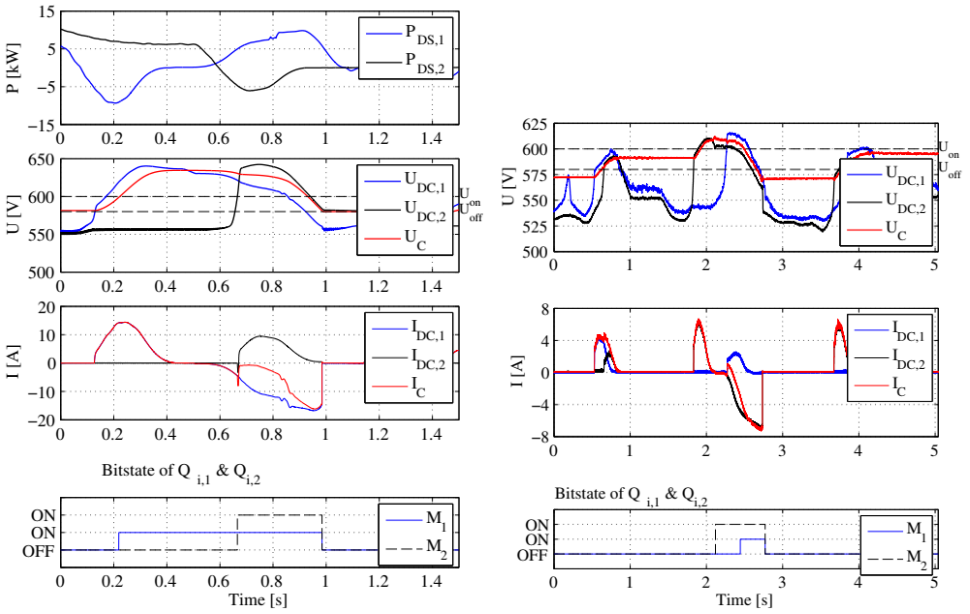

Fig. 2.9. Comparison of interconnection operation examples in a modelled (right) and experimentally measured system (left).

The obtained data allowed further system optimization. As observed, for example, actual U_C voltage reaches a value lower than U_{OFF}, demonstrating the time delay in real system semiconductor switching operation, and has been the subject of more extensive analysis (the author's Publication 16).

Development of a modular system prototype

Given the expected use in an industrial environment, where it would be necessary to organize the energy exchange between individual industrial robots on a similar scale to that achieved from an actual production plant, it is concluded that the typical number of robots placed together is up to five units. This type of electrical equipment would be used to optimize the operation of one production cell by modifying existing robots. Based on the data obtained and the model produced, an analysis was developed to build a system of five robot machines using modelling tools, as well as a practical modification of the design of the prototype taking into account the necessity of a modular system.

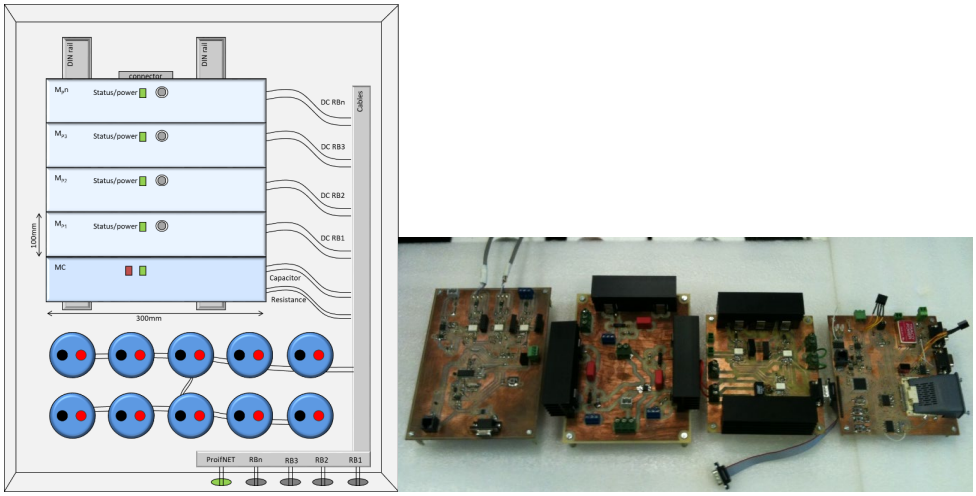

Fig. 2.10. Conceptual sketch of the principle of modular system approach (left) and first prototypes of functional modules (right).

Figure 2.11 shows the realization of the equivalent model of the system in the Simulink environment to determine the operating modes and associated electrical parameter values of the electrical system.

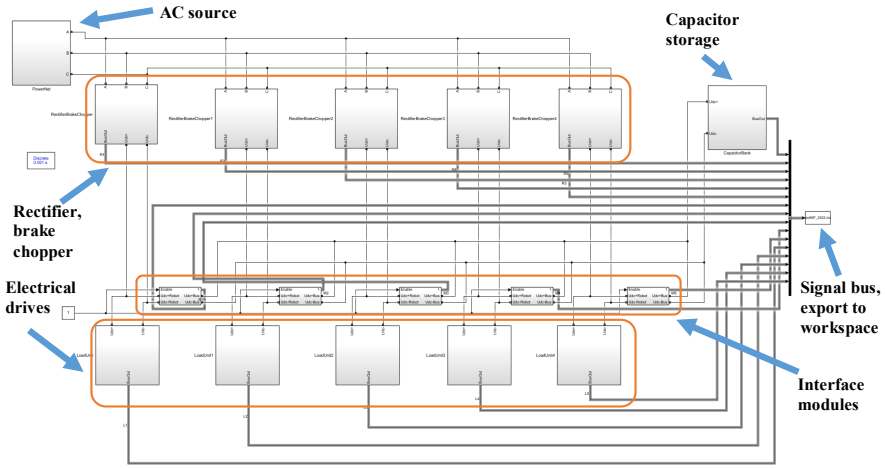

Fig. 2.11. Model structure for five interconnected industrial robot operational analysis.

Modelling results allow to explore interconnection module switching processes and the impact on overall system operation. Figure 2.12 shows part of the data obtained, graphically representing the voltage dynamics of individual DC buses.

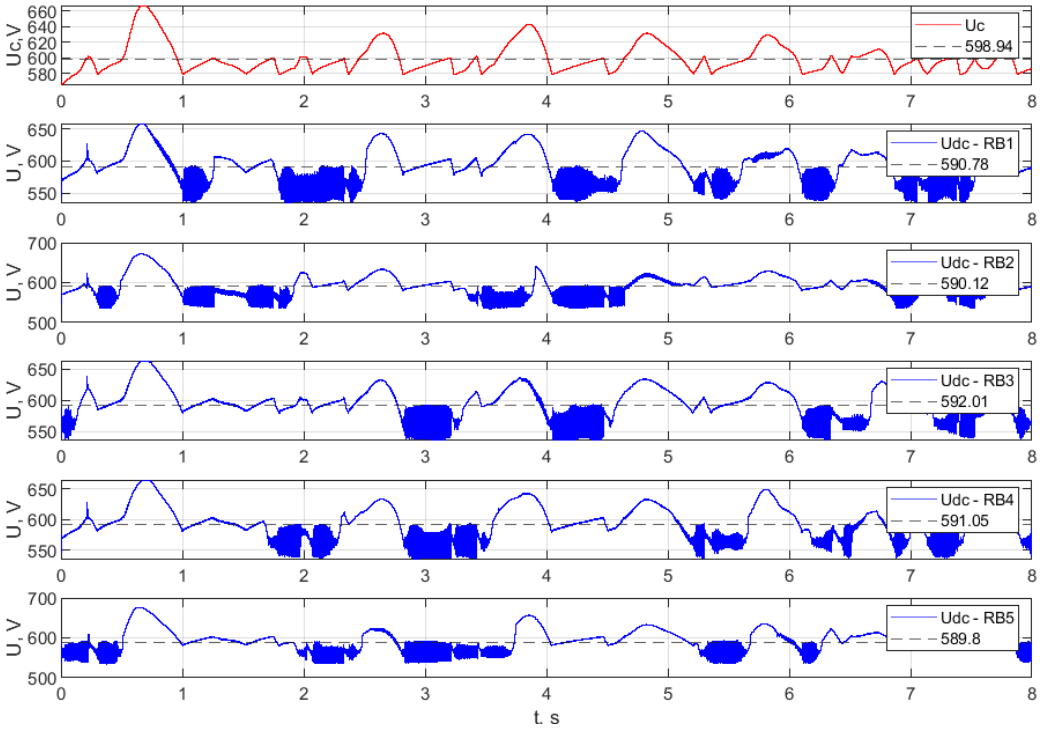

Fig. 2.12. Example of modelling results for the 5-module system – dynamics of individual DC bus voltages.

The choice of transistors and diodes for selected main semiconductor elements was also optimized by studying the appropriate thermal processes, as well as the galvanic insulation of module housings and the ability to combine on single radiators for passive cooling applications.

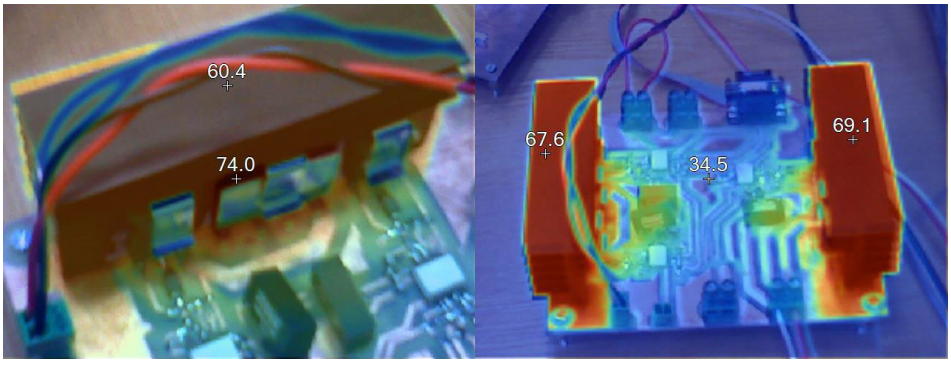

Fig. 2.13. Example of a thermal process identification and testing process with increased power to determine critical temperatures during the design of the equipment.

A version was created in the course of successive development of the solution envisaging the assembly and housing design for the equipment taking into account typical installation

conditions for electrical and automation equipment in cooperation with Daimler AG. Figure 2.14 shows the design of the installation solution and the modules created using 3D CAD software.

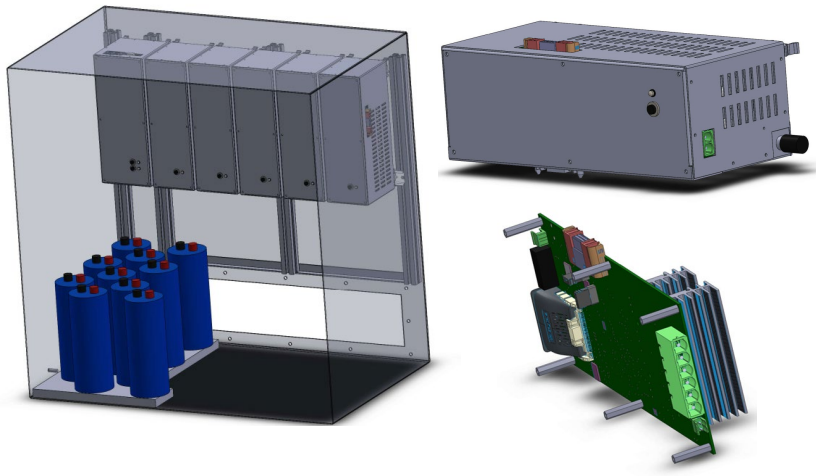

Fig. 2.14. The concept of modular installation assembly and practical implementation of modules in a CAD environment.

A real prototype of the equipment was built (see Fig. 2.15) taking into account the aspects of optimization and modular system described above for industrial applications in the production plant.

Fig. 2.15. A practically implemented modular solution for the DC link interconnection of industrial robots.

3. ANALYSIS OF INDUSTRIAL ROBOT APPLICATION WITHIN LABORATORY SCALE DC MICROGRID

The practical implementation of a DC microgrid for experimental power flow analysis of a few industrial robot applications and possible combinations with energy storage and renewable power infeed has been of interest to Riga Technical university (RTU) Institue of Industrial Electronics and Electrical Technologies. Efforts and related author's findings regarding the implementation of DC testing laboratory are represented in the author's Publications 3, 4, and 8–14.

Interest in physical DC grid implementation as testbed for new converter prototypes and system operation analysis at RTU has aligned with the European Union research project AREUS objectives for the demonstration of market-available DC technologies for industrial DC grid installation and future developments needed. Figure 3.1 represents the top view layout of the RTU AREUS Demo laboratory room at its final setup:

1 – active AC/DC rectifier unit (55 kW);
2 and 3 – universal robot load emulator units (23 kW);
4 – lithium ion battery energy storage system (BESS) 16-22 kW;
5 – supercapacitor storage system (30 kW);
6 and 7 – 600 V DC-Robot prototype and KUKA DC robot controller cabinet with a load of 21 kW;
8 – master PLC controller (cell controller);
9 – solar DC/DC converter (3–4 kW) for 3.3 kW solar panel array;
10 – optional wind energy emulator setup.

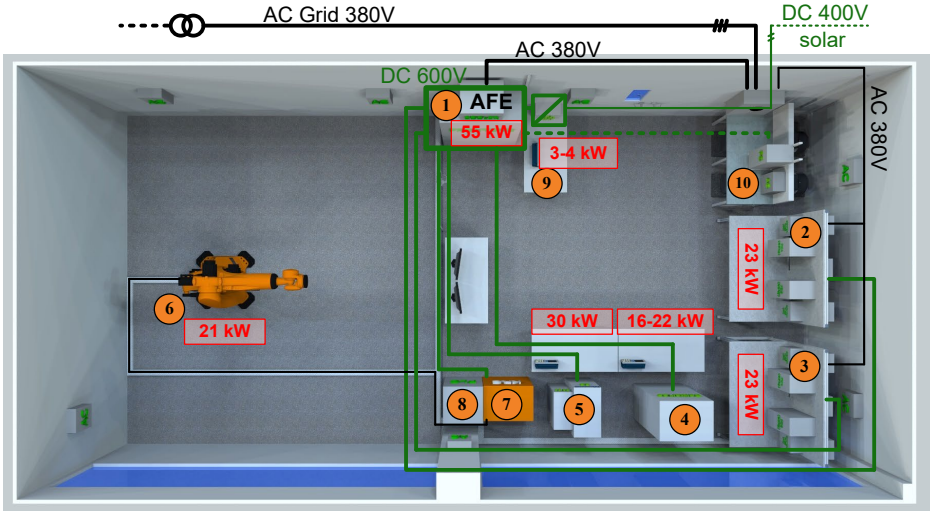

Fig. 3.1. RTU DC microgrid laboratory setup (also referred to as AREUS Laboratory).

The following DC microgrid design aspects and challenges for experimental DC microgrid laboratory implementation have been solved and covered in the Thesis.

- Dynamic DC power flow operation demonstration resembling three industrial robots within limited floor space.
- Implementation of synchronous multipoint power flow measurement solution for experimental data logging and analysis.
- Operational behaviour analysis of central bidirectional AC/DC power interface – also called active front-end converter for DC microgrid supply.
- Cyclic manufacturing process operation analysis and possible optimization measures of electrical equipment.

Development of DC power flow emulator

The small-scale industrial microgrid laboratory environment is foreseen as a physical model of multiple industrial robot installations for manufacturing task execution. Combination of the main task for several dynamic DC load unit implementation along with given constraints of available floor space, investment budget and research areas of IEEI institute allowed to make the decision on the arrangement of an electromechanical system of coupled induction type electrical drives (see Fig. 3.2), combining torque and speed controlled drives for overall system operation objective of controlled DC side power flow.

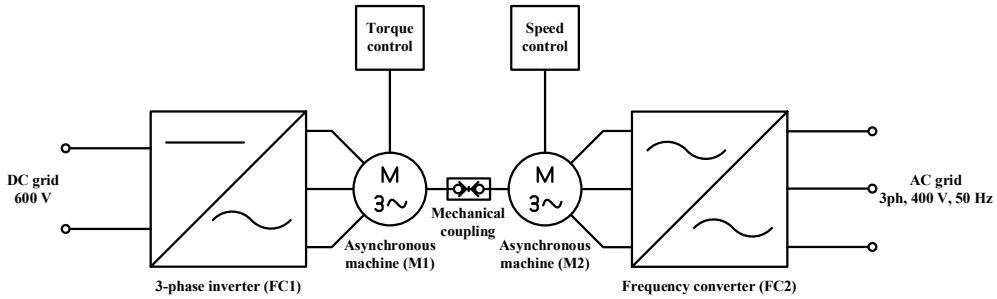

Fig. 3.2. Principal schematic of the bidirectional DC power flow emulator.

Motor drive frequency converter FC2 has an objective of maintaining the stable rotational speed of the coupled system. The other frequency converter, FC1, is operated by an external torque reference provided by the user related to DC power flow demand. Both frequency converters are identical market-available ABB ACS series 22 kW drives, and one of the units is directly supplied by the DC microgrid bypassing input rectifier. The main control principle of DC side power flow control is related to the proportionality of a given torque command, provided mechanical power and respective electrical power consumption or generation as described by Eqs. (3.1)–(3.3).

$$P_{M1} = T_{M1}\omega = \frac{T_{M1} \times n}{9.550} \tag{3.1}$$

P_{M1} is the output mechanical power of electrical machine M1 and the respective mechanical torque T_{M1} by given rotational speed of the linked motor shafts n. If the speed of the linked shafts is kept constant, the desired electrical power flow P_{DC} can be correlated to the necessary torque setpoint. However, the physical system also has losses that can be combined into a single

quantity, ΔP, according to Eq. (3.2) and respective power flows for motoring and generation modes, as represented in Fig. 3.3.

$$\Delta P = \Delta P_{FC1} + \Delta P_{M1,el} + \Delta P_{M1,mech} \tag{3.2}$$

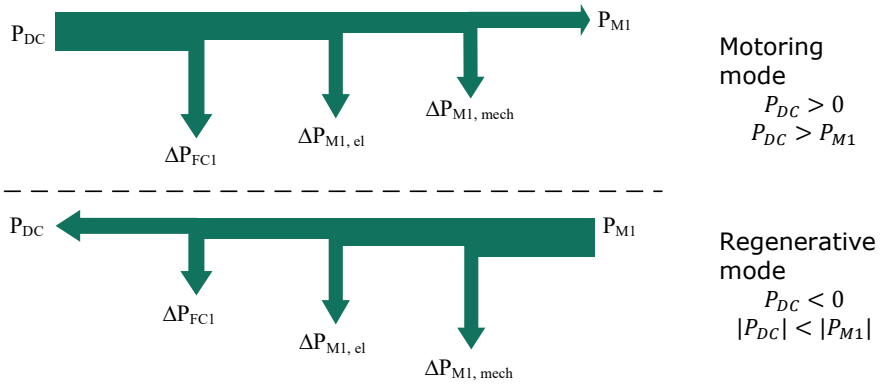

Fig. 3.3. Electrical power flow in motoring (top) and regenerative (bottom) modes.

The exact power balance of DC side connected electrical drive M1 is as in Eq. (3.3).

$$P_{DC} = P_{M1} \pm \Delta P \tag{3.3}$$

A controller has to be developed to dynamically change the torque reference according to the desired DC power flow profile. Since several parameters can vary during operation (speed fluctuations, system losses being dependent on temperature, load conditions, power flow, etc.), a closed-loop controller for calculation of compensated torque reference for the drive FC1 based on the demanded and the measured DC bus power values and the energy losses has to been proposed Fig. 3.4.

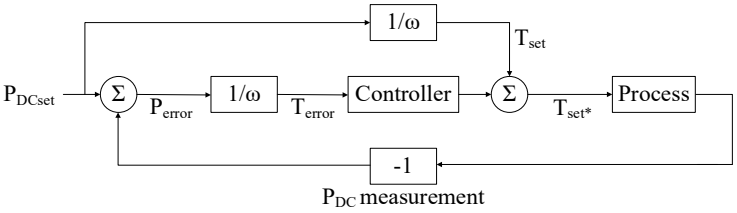

Fig. 3.4. Proposed controller structure for dynamic DC power flow emulation by electrical drive torque variation.

The controller has to compensate only for relatively small deviations from the desired output. In the case of the DC power flow controller feedforward torque reference T_{set} approach based on dominant system behaviour according to Eq. (3.1) is beneficial. The difference between the set and the measured power value is caused by the electromechanical losses present in the system. The task of the controller (Fig. 3.5) is then to modify the torque reference for the compensation of these losses for the final drive arrangement, as represented in Fig. 3.6.

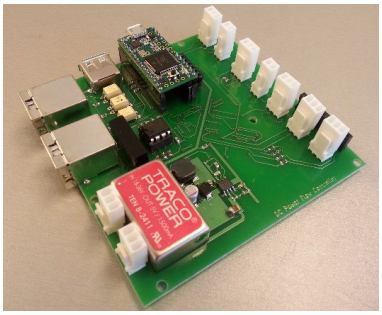
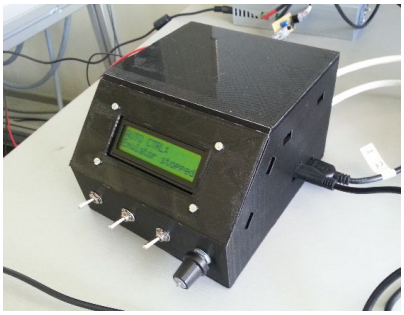

Fig. 3.5. DC power flow emulator controller PCB and enclosure.

Fig. 3.6. DC power flow emulators developed in the RTU AREUS demo laboratory.

The final operating parameters regarding DC power flow physical emulation capabilities are summarized in Table 3.1.

Table 3.1

DC Power Flow Emulator Performance Parameters

DC power ratings	P_{DC} (regenerative)	–18 kW
	P_{DC} (motoring)	+22 kW
Power flow dynamics	dP/dt (regenerative)	–378 kW/s
	dP/dt (motoring)	+448 kW/s

The comprehensive development procedure for the described bidirectional power flow emulator system has been presented in the author's Publication 11. Potential alternatives for

drive control approaches based on funnel controller [24] with respect to a given application have been presented in Publication 14.

Analysis and modelling of an active front-end AC/DC converter

The AC/DC electrical interface converter for bidirectional power exchange between 600 V DC local industrial microgrid system and existing AC infrastructure has been utilized in order to apply power flow conditions similar to those in real production processes.

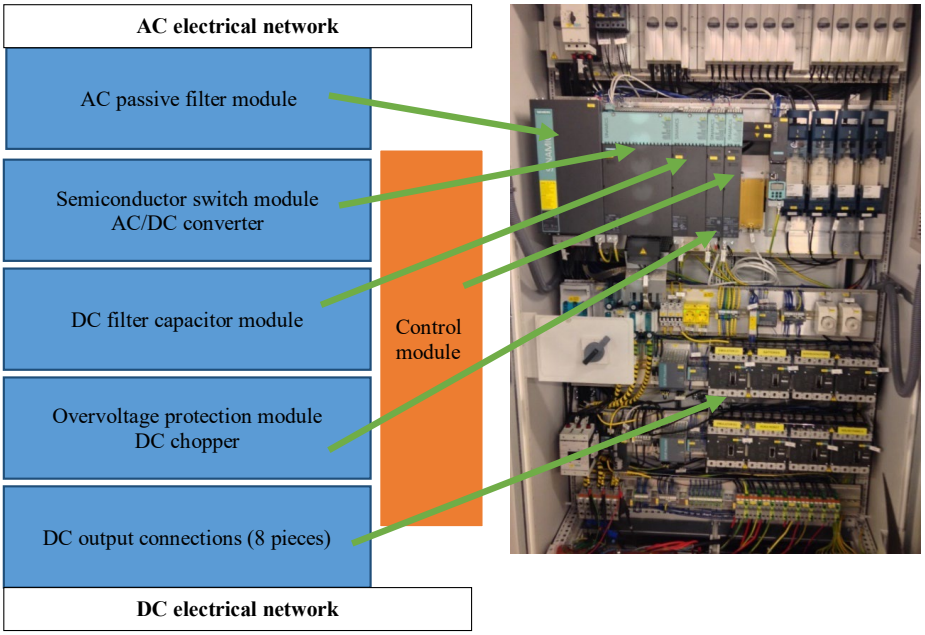

Fig. 3.7. Physical setup of an AC/DC interface converter (right) and a functional block assembly structure (left)

Electrical equipment is based on industrial-grade components selected for specific prototype operation according to planned DC demonstration activities within the AREUS project framework. The significance of a central AC/DC interface converter for DC microgrid requires estimation by measurements of both AC and DC side-related electrical system operating conditions as well as typical characteristics being efficiency, power quality and similar quantities. The idea of a generalized converter operation model extraction based on physical measurements has been applied, since the model-based DC grid design approach has been of interest for future development and practical applications in industry and research environments.

Experimental testing methods

In order to evaluate the performance of AC/DC electrical interface equipment, an electrical system for bidirectional power flow operation has been developed. Electrical testing within the power range of 40 kW for energy consumption and generation with respect to the AC electrical

system has been done. The schematic arrangement using two electrical power flow emulation units has been connected as presented in Fig. 3.8. Electrical power measurement has been done with high-precision power analyser equipment. Two DC-side electrical power flows have been measured with N4L PPA3300 power analysers connected with electrical drive setup for energy flow operation as shown in Fig. 3.9.

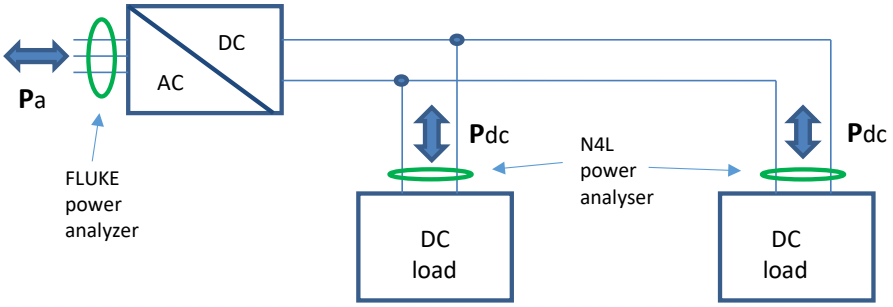

Fig. 3.8. The structure of AC/DC converter operation measurement setup.

Fig. 3.9. FLUKE 434 Series II installed for AC-type electrical measurements (left) and N4L PPA3300 power analyser and DC electrical power flow emulator in the background (right).

The presented testing arrangement has been operated at various load or generated power levels within a range from –36 kW (generating) to 45 kW (loading). The following operational performance indicators have been obtained at various power levels.

Efficiency has been obtained by observing power measurements on both sides of the AC/DC converter and their respective ratio according to power flow. Negative DC power represents operation feeding energy to AC grid, whereas positive energy is drawn from the AC grid. The converter efficiency has been obtained within the range of –36 kW to 45 kW. The efficiency reaches values higher than 0.9 in a broad operating range, exceeding 5 kW for both consumption and regeneration.

Power factor represents the ability of equipment to utilize electrical infrastructure efficiently and consume active power without reactive power component. The ideal case of power factor reaching a value of 1 means that pure active power has been drawn from AC grid. In the case of regeneration to AC grid, the respective ideal power factor value is –1.

The respective efficiency and power factor results related to the DC side power flow are presented in Fig. 3.10.

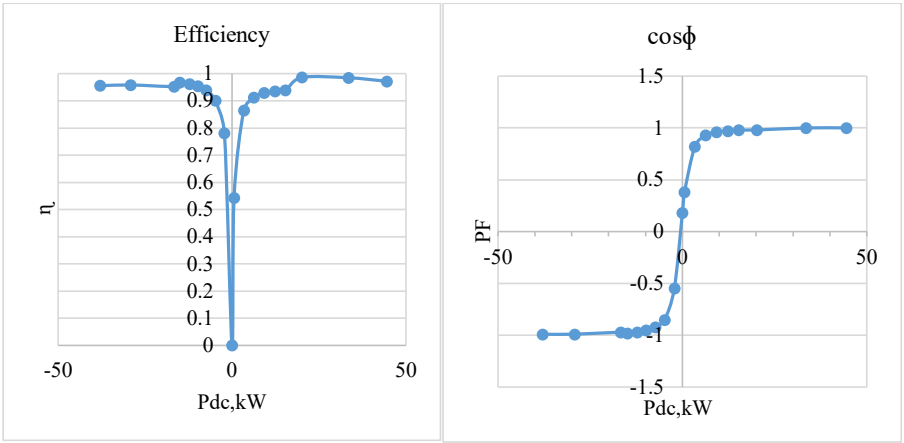

Fig. 3.10. AC/DC converter efficiency and power factor related to DC side power.

Total harmonic distortion factor (THD). The nominal frequency of AC power system is 50 Hz, therefore, the AC waveforms of voltage and current ideally should have only 50 Hz sinusoidal character. In real applications, other harmonics or base frequency multiples are present, adding additional losses and reducing electrical power quality parameters. A parameter known as total harmonic distortion factor (THD) represented in percent allows evaluating the harmonic content of voltage or current. Ideally, the value of THD should be 0 if only the base frequency is present in the analysed waveform. It can be observed that the current waveform quality is significantly reduced at light load conditions, as represented in Fig. 3.11.

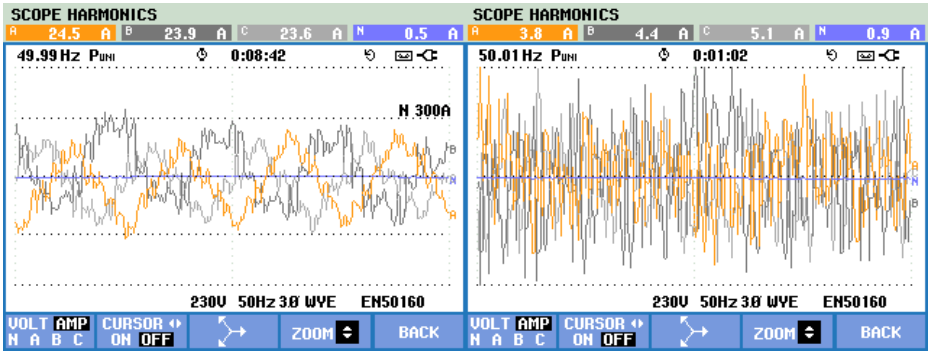

Fig. 3.11. AC phase current waveforms at P_{DC} = 15.3 kW, average current 24 A (left) and P_{DC} = –2.2 kW, average current 4.5A (right).

The results of harmonic analysis and THD coefficient estimation for both waveforms are depicted in Fig. 3.12.

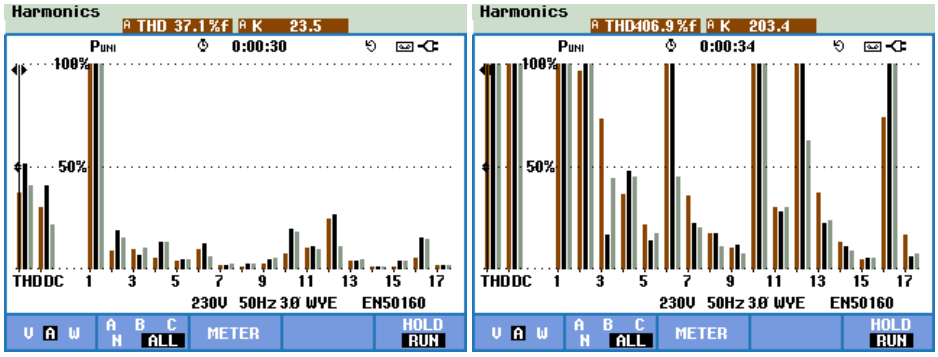

Fig. 3.12. AC phase current harmonic analysis at P_{DC} = 15.3 kW, average current 24 A (left) and P_{DC} = –2.2 kW, average current 4.5 A (right).

The obtained operational behaviour has been measured and represented in Figs. 3.13 and 3.14, where significant variations of AC side current waveforms at light load conditions are represented, whereas voltage distortion is less significant.

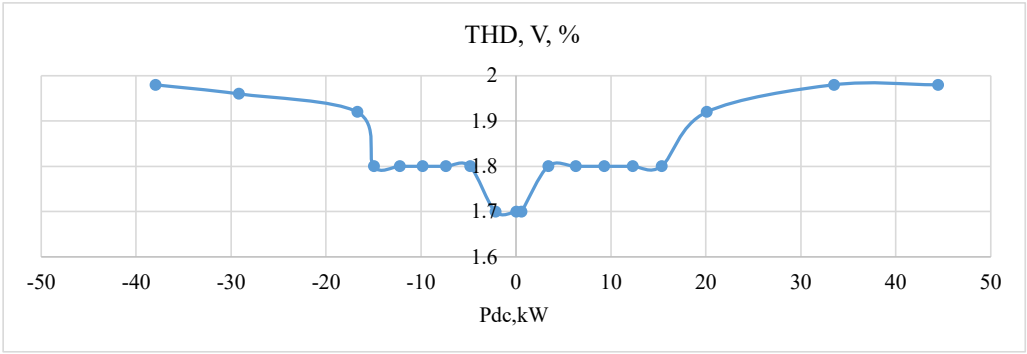

Fig. 3.13. The obtained voltage THD variation referred to DC side power flow operation.

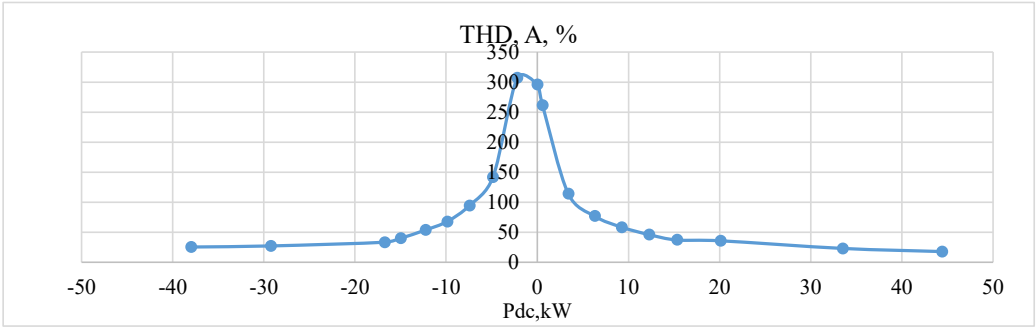

Fig. 3.14. The obtained voltage THD variation referred to DC side power flow operation modelling of AC/DC converter.

DC side measurements

For DC side operation behaviour analysis, AC/DC converter has been operated at various load and recuperation power levels enabled by the DC power flow emulator equipment described

before. Voltage and current waveforms have been obtained through the DataTranslation DAQ acquisition module with a maximum sampling frequency of 44 kHz. The following figures Figure 3.15 represents time and Fig. 3.16 – frequency, which represent the AC/DC converter performance.

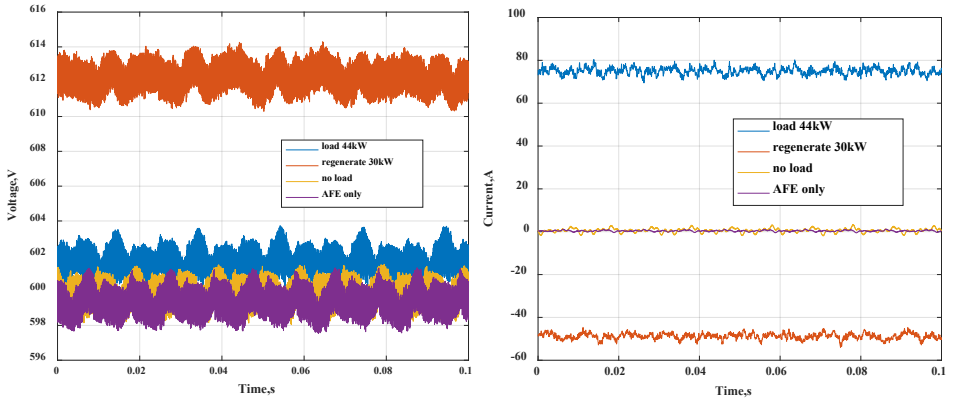

Fig. 3.15. DC link voltage and current waveforms at DC link terminals of AFE converter in time domain.

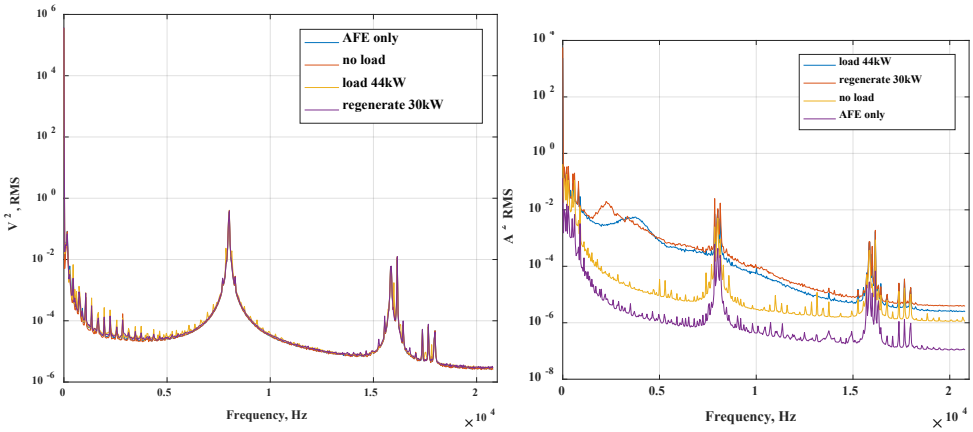

Fig. 3.16. Frequency content analytical results of DC terminal voltage and current at various load states.

The obtained data represent the presence of fundamental 8 kHz AC/DC converter switching frequency and variation of DC side voltage by an increase of 10 V by reversed power flow operation. The spread of the obtained spectrum of current waveform at higher load conditions is observed, and significant multiples of fundamental switching frequency are identified for better design of related measurement equipment and related signal filtering needs. The requirements of DC-related frequency content and related EMC issues is one of the areas being discussed in Publication 8, and while some standards are applicable already, for example, of PV related LVDC systems, many aspects have to be included in future standardisation activities [25], [26].

Development of a simplified model of AC/DC unit.

Based on available data, an approach for the respective AC/DC converter model development has been implemented and described in Publications 9 and 12. Pulsed load testing for voltage dynamic variation on DC bus has been done with a step load variation of 6.5 kW. The simplified dynamic model has been designed according to the structure presented in Fig. 3.17.

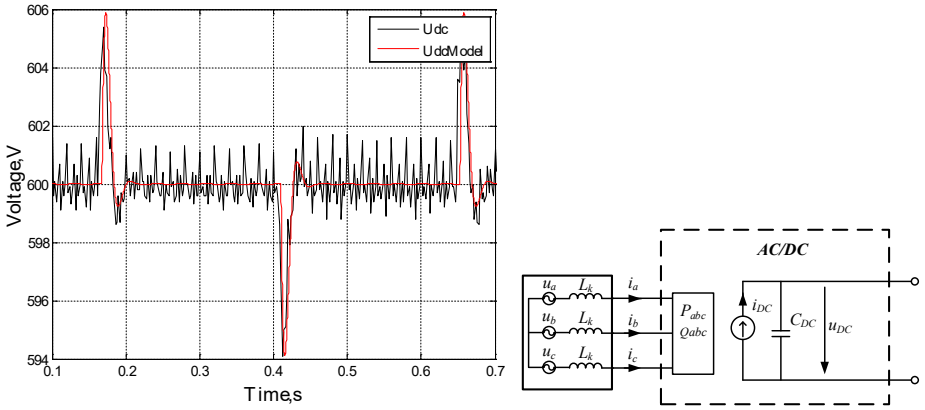

Fig. 3.17. Actual and modelled DC bus voltage dynamics (left) and implemented model structure (right).

The basic principle is the current source control feeding current into a capacitor representing the 4.1 mF output filter capacitor. The reference voltage of the capacitor is set 600 V, representing the microgrid nominal voltage. The charging and discharging of the capacitor have been controlled by the PI-type controller observing output voltage with respect to the reference voltage and respective current source implementation. Other aspects, such as AC and DC side power balance and converter losses, have been based on an approximation of the previously described efficiency and power factor data obtained by measurements.

Application of a synchronized power flow measurement system

In order to perform synchronized power flow measurements for AC and DC-based electrical supply systems, a set of measurement devices has been developed and introduced within the laboratory and industrial DC supply infrastructure. The motivation for applying customized power measurement equipment is related to immediate and time-coordinated data collection needs and future extension for data transfer via industrial communication networks such as Profinet. The ever-expanding relevance of non-sinusoidal, bidirectional, AC and DC-based power flows in real electrical installations demands low-cost distributed power monitoring and measurement solutions. Previous research activities have led to a novel power flow measurement approach utilizing non-even time sampling [27].

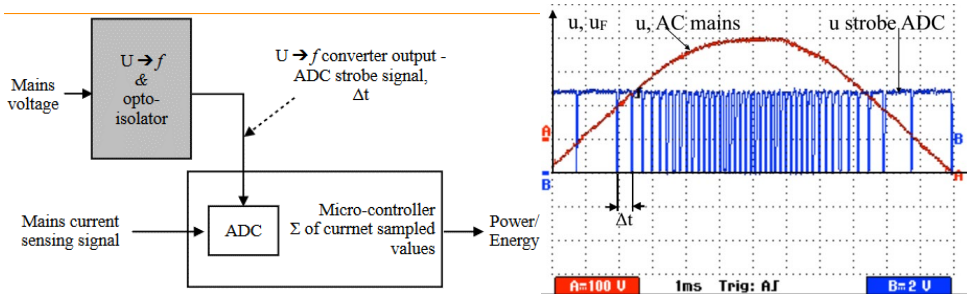

Fig. 3.18. Working principle of a voltage-controlled variable oscillator-based sampling system [27].

The approach is to utilize a variable frequency oscillator for sampling that corresponds to an instantaneous measured voltage *u* by linear function *K,* as in Eq. (3.4):

$$f_{sample} = Ku \tag{3.4}$$

The sampling frequency determines integration time periods *Δt* for energy calculation, as in Eq. (3.5).

$$\Delta t = \frac{1}{f_{sample}} = \frac{1}{Ku} \tag{3.5}$$

Energy calculation within the determined time period *T* is obtained according to the function of Eq. (3.6):

$$\mathrm{W} = \sum_{0}^{T} p\Delta t = \sum_{0}^{T} ui\Delta t \tag{3.6}$$

Since periods *Δt* are related to the variable sampling process in linear relation to voltage, the equation can be rearranged according to Eq. (3.7):

$$\mathrm{W} = \sum_{0}^{T} ui\Delta t = \sum_{0}^{T} \frac{ui}{Ku} = \frac{1}{K}\sum_{0}^{T} i \tag{3.7}$$

Based on the presented principle, a set of measurement devices has been designed for application in industrial microgrids and analysis for individual manufacturing equipment units and respective electrical power flow. Since various types of electrical connection technologies and methods are present in real installation, electrical power flow metering equipment has been adapted for both integrated and external current measurement solutions. Industrial robot electrical power metering units have been implemented as extension cables for existing industrial connectors being used, as shown in Fig. 3.19.

Fig. 3.19. Power flow meter as industrial robot extension cable.

An integrated DC power flow measurement device set has been applied with an internal current measurement sensor. Higher power level measurements and 3-phase arrangement have been achieved by measurement devices with external current measurement clamps, as shown in Fig. 3.20. Additional communication modules for optical data transfer and industrial data protocol standard Profinet are integrated within the same device.

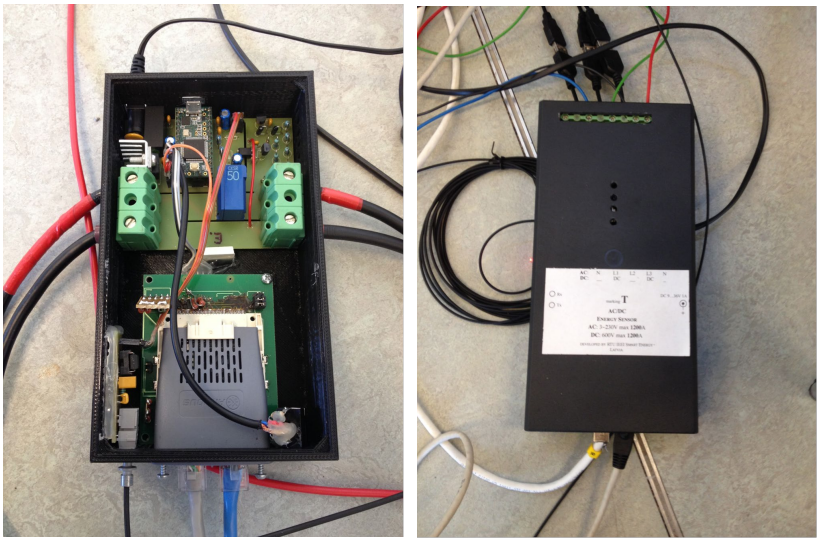

Fig. 3.20. Power meter with integrated current measurement and external current clamps.

In order to achieve time-synchronized and consistent data of distributed power flow measurement installation, optical data communication has been implemented. Figure 3.21 represents a central optical fiber connection for centralized data acquisition.

Fig. 3.21. Optical fiber data transmission and aggregation device.

The synchronized data set is produced by aggregating individual metering unit data with a bidirectional optical communication data network, providing synchronous requests for every power flow meter every 20 ms. Internally, each power meter unit has a sampling frequency of 2.8 kHz and provides an averaged value on request for the previous 20 ms acquisition time period.

Cyclic operation-related parameter analysis

As laboratory scale installation of DC microgrid is physically implemented, respective analysis of system operation and related selection of protection equipment or power supply dimensioning has been of interest. Significant property within industrial manufacturing operations is related to the cyclic repetition of automated processes and respective electrical power consumption dynamics.

Typically, the data with a given sampling frequency f_{sample} for a respective period time frame with length t_n is available from measurements or simulations. An approach for input data analysis based on the sliding analysis window concept along extended operational period data has been applied. The sliding analysis window being shifted along the whole dataset and with variable window width can provide a method for data categorization or time-related distribution analysis as presented in Fig. 3.22.

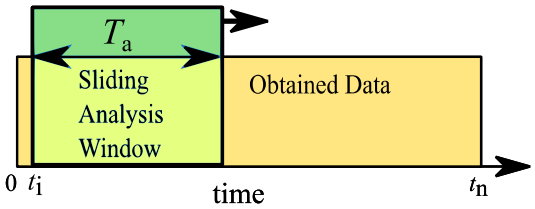

Fig. 3.22. Visualization of sliding analysis window approach application for power data analysis.

The presented idea is applied for dynamic power variation analysis to retrieve an overview of the characteristic behaviour of electrical load maximal instantaneous power requirement and respective combined power demand for a group of loads (the author's Publication 8).

Therefore minimum and maximum sliding window size options can be defined based on Eqs. (3.8) and (3.9).

$$T_{min} = \frac{1}{f_{sample}} \tag{3.8}$$

$$T_{max} = t_n \tag{3.9}$$

The minimum analysis window is defined by an applied sampling frequency of data and the respective distance in time between two adjacent samples. The maximum window available for analysis is limited by the total data sampling time frame t_n. By variation of window size, T_a, the respective number of following samples for evaluation within the analysis window can be defined according to Eq. (3.10).

$$n = \frac{T_a}{f_{sample}}, T_a \in [T_{min}, T_{max}] \tag{3.10}$$

Evaluation of average power P_{avg} within the scope of analysis window being shifted according to the number of samples i is represented by Eq. (3.11).

$$P_{avg}(i, T_a) = \frac{1}{n}\sum_{i}^{i+n} P_i, i \in [1, t_n - n] \tag{3.11}$$

The final analysis result for a particular analysis window width being shifted along initial data is determined according to Eq. (3.12).

$$P(T_a) = \max(P_{avg}(i, T_a)) \tag{3.12}$$

By analysis according to equations, the characteristic behaviour of electrical load instantaneous peak power requirement can be determined, as given in the example.

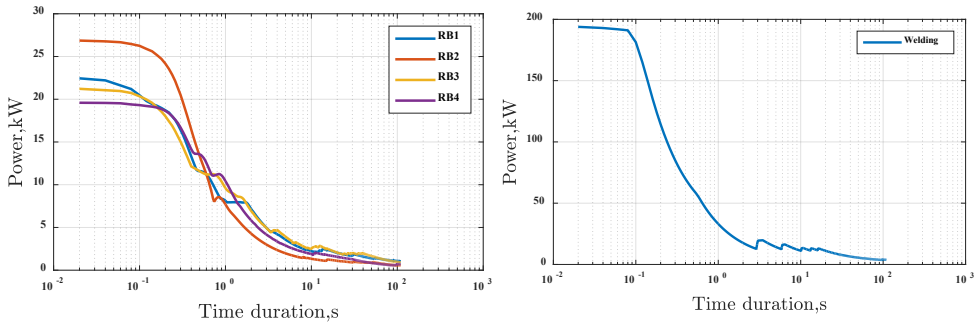

Fig. 3.23. Peak power analysis results of a 4-manipulator set (left) and the welding process (right).

The analytical approach has been further applied for interconnected DC microgrid peak power rating and respective infeed converter power rating selection. The following graphical workflow in Fig. 3.24 represents two approaches based on available information if only individual electrical unit power profiles are available or information about combined system behaviour and time-based coordination is available.

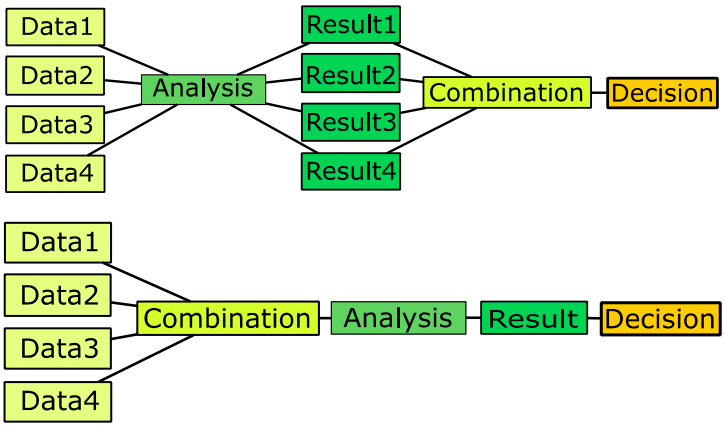

Fig. 3.24. Comparison of the parallel power peak demand analysis approach (top) and the combined approach (bottom).

The obtained results represent a significant variation of achieved peak power demand character, and therefore, the significance of system modelling needs in advance for the electrical system and component dimensioning.

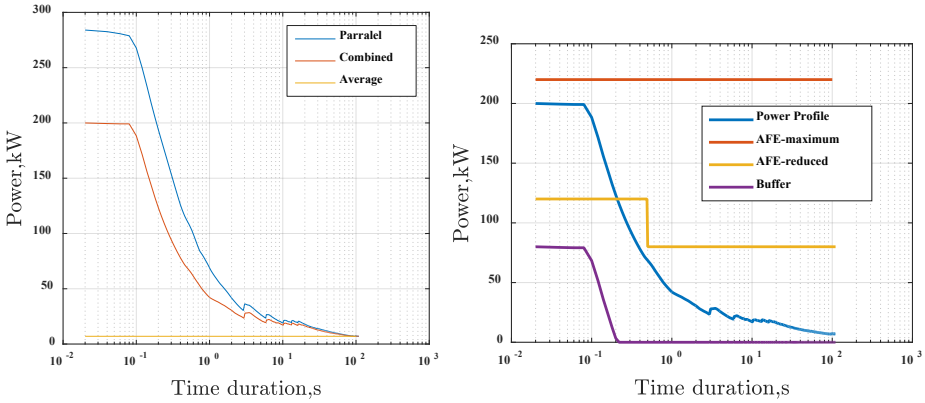

Fig. 3.25. Parallel and combined analysis result for power demand (left) and potential converter dimensioning scheme with dynamic energy buffer application (right).

A similar approach has been applied to analyse industrial robot cyclic current profiles (Publication 10). The interest in individual unit current flow behaviour analysis has been related to the optimal selection of appropriate circuit protection rating as well as the identification of unique patterns for each robot for diagnostic application in future. In combination with semiconductor-based circuit protection developments [28], an adaptive approach for critical parameter adjustment can be considered. Current reference profiles are used as input data set of industrial robot, as represented in Fig. 3.26.

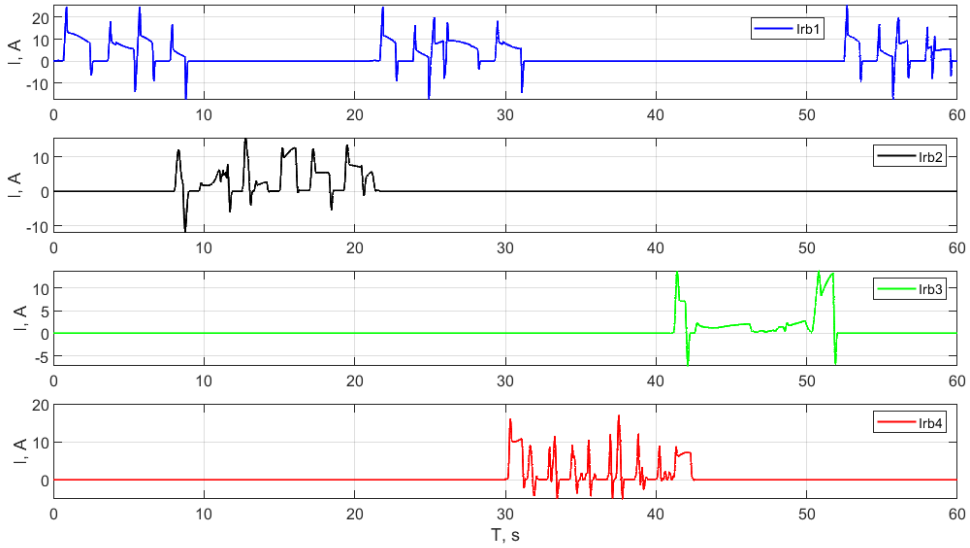

Fig. 3.26. Example of a 60-second repetitive industrial production cycle and consumer electrical load current profiles in the case of four industrial robots assisting for several operations: IRB1 – material handling; IRB2 – to carry a welding gun; IRB3 – to carry a glue dispenser; IRB4 – to carry clinching equipment.

The analysis of peak average values of the current concerning time duration has been represented in and compared to a few typical fuse characteristics available in datasheets for PV and general type loads.

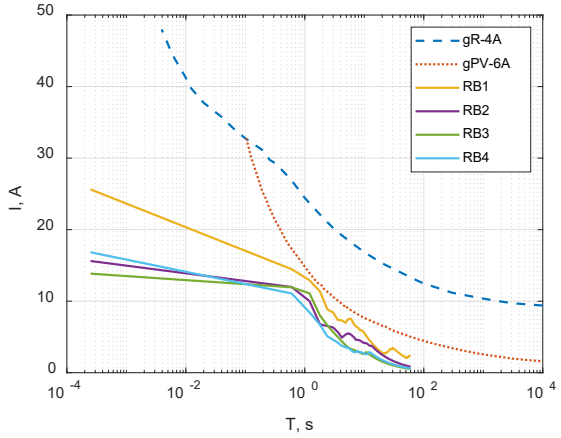

Fig. 3.27. Comparison of the sliding window analysis for highest mean current values and the typical fuse current-time curves of types gR-4A and gPV-6A.

Another approach has been carried out using the sliding window approach for categorization of obtained measurement sample data within categories C of measured values x. In this way the total operation period time span from 0 to final sample t_n has been assigned according to

respective sample measurement values to categories from C_1 to Cn covering the whole measured current profile value range.

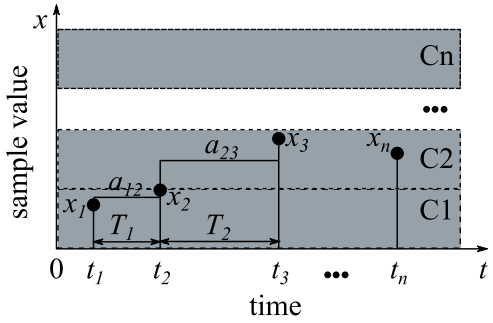

Fig. 3.28. Graphical representation of current sample *x* categorization analysis within classes C.

Such an approach has been considered for future operation online observation and application that would generate patterns for each individual robot operation within a given manufacturing cycle. If cycle time is fixed, then the analysis pattern result obtained by the logged current profile would also represent similarity. Fig. 3.29 provides a graphical representation of load current behaviour.

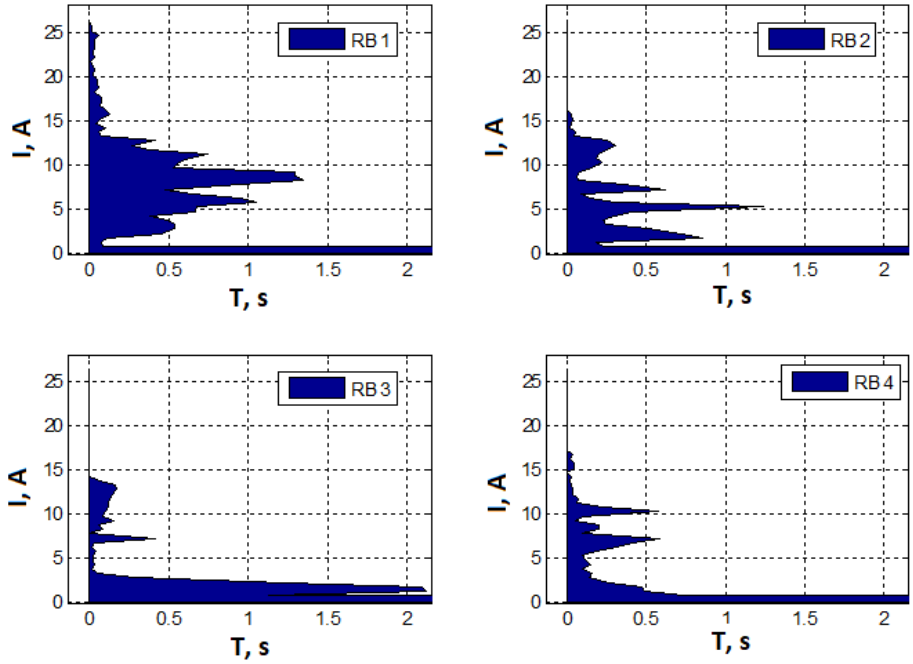

Fig. 3.29. A magnified view of analysis results for time span below 2 seconds.

4. EXPERIMENTAL TESTING OF AN ENERGY EFFICIENT DC MICROGRID IN A LABORATORY AND A ROBOTIC AUTOMOBILE MANUFACTURING INSTALLATION

Implementation of robotic manufacturing DC microgrid for automotive production

For experimental verification of DC microgrid-related equipment and demonstration of available state-of-the-art technologies, a new purpose-built DC microgrid installation has been implemented by Mercedes-Benz AG (previously Daimler AG) company in a factory located at Sindelfingen, Germany.

Joint research and development activities have been pursued together with Riga Technical university within AREUS research project; therefore, the availability of an industrial DC system for operation analysis has been valuable, as represented in the author's Publication 5. Within the implementation of the AREUS project, an installation referred to as the AREUS DC demo cell was designed, commissioned, and used for experimental verification. Since the company Mercedes-Benz AG has know-how and experience in automobile manufacturing and respective automation infrastructure development, a new DC electrical system has been implemented according to the typical approach of continuous automotive production process distributed into separate areas referred to as production cells.

The design and functionality of a particular DC demonstration cell have been based on the following objectives and background motivation aspects, the main of those being:

- to copy a part of the actual manufacturing process and demonstrate a design for the conversion of AC-based electrical supply infrastructure to DC-based electrical supply infrastructure;
- to apply existing technology and automation standards and guidelines implemented by Daimler AG globally in a series of factories;
- to incorporate several technology tools and joining technologies for car body production and carry out respective equipment adaptation for DC-supplied operation;
- to obtain knowledge of market-available DC electrical equipment and supplier base and identify technological solutions to be developed in future.

As a result of defined objectives single existing production cell design dedicated for assembly of several prefabricated metal parts into single part for futher processing has been selected. Primary operations are carried out by a group of four industrial robot manipulators combined with spot welding, rivet punching, and adhesive bonding as applied production technologies. The physical installation has been presented in Fig. 4.1.

Fig. 4.1. DC microgrid realization as an automotive manufacturing cell for experimental analysis (Publication 5).

A DC microgrid cell has been built within a square area of around 10 meters side length and separated by a safety fence. Industrial robot controllers and other electrical technology equipment cabinets have been placed along the border, and the DC electrical supply rail has been implemented as a ring type busbar raised above the safety fence. Figure 4.2 represents a combination of applied equipment and related measurement locations for data collection of power flow analysis by spatially distributed power flow measurement equipment installed by RTU.

System component overview

Key system components of DC microgrid cell are:

- active front-end AC/DC converter unit (AFE) of rated power 450 kW assembled by industrial energy conversion modules;
- a set of four industrial robots KUKA KRC4, 210 kg payload manipulators;
- li-ion battery with interface converter of rated power 30 kW;
- PV infeed DC/DC converter;
- electrolytic capacitor bank, 132 mF;
- technology tools adapted for DC operation (spot welder, rivet punch tool, glue dispenser, rotating conveyor table).

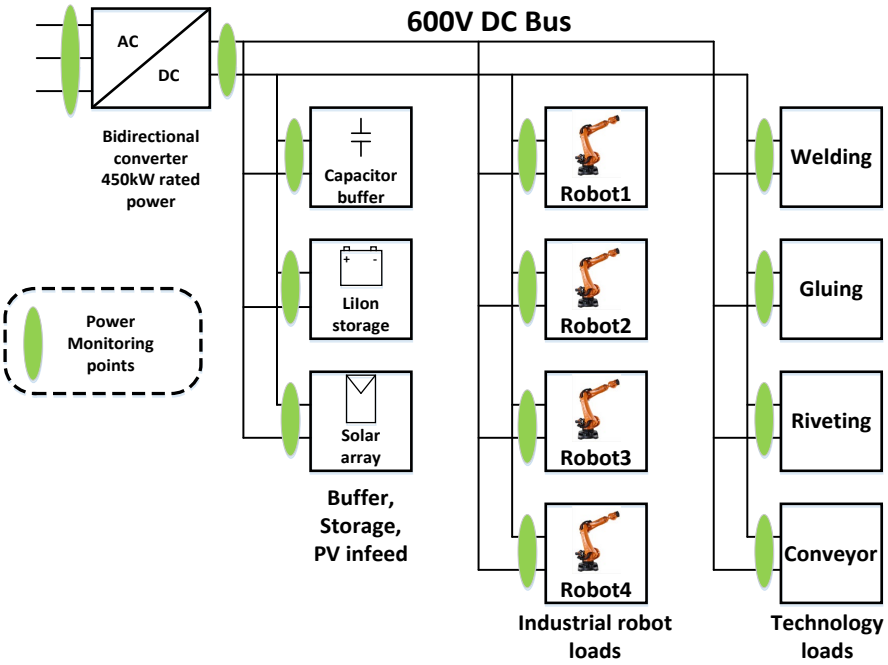

Fig. 4.2. Structure of examined DC microgrid for automotive manufacturing application.

The available setup has been utilized for several experimental tests of power and energy-related performance estimation of industrial application DC microgrid systems.

Individual robot unit test

- Conversion of industrial robot power supply from AC to DC and related energy efficiency variation.

DC microgrid operation test

- Estimation of reused energy potential in industrial application of individual units.
- Dynamic effects of high peak power demand operation.
- Estimation of the power balance of DC-type microgrid system and central interface converter performance.

Analysis of individual robot's operation by converting the control cabinet from AC to DC supply.

In this series of power flow measurements, a physical substitution approach of industrial robot control cabinets of type KUKA KRC4 from conventional AC-based products to DC-based protoype designs has been applied. Since the applied power flow measurement equipment has the capability of both AC and DC type electrical power data acquisition, the same devices are used and designed explicitly for industrial robot cabinet KUKA KRC4 electrical interconnection needs, as described in the previous chapter. Measurements were taken during the production process, and it was observed that the motion type of robots varied due to the

position of individual parts used for assembly. The parts are supplied stacked vertically and pick-up time is increasing, since the following part has to be picked up at lower position than previously. A typical completed production cycle length of 98 seconds for all four industrial robots has been obtained for AC to DC cabinet conversion analysis.

Fig. 4.3 represents a graphical comparison of power flow profiles of industrial robots within the production cell of the combined four industrial robot operations for AC and DC-type electrical supply use cases.

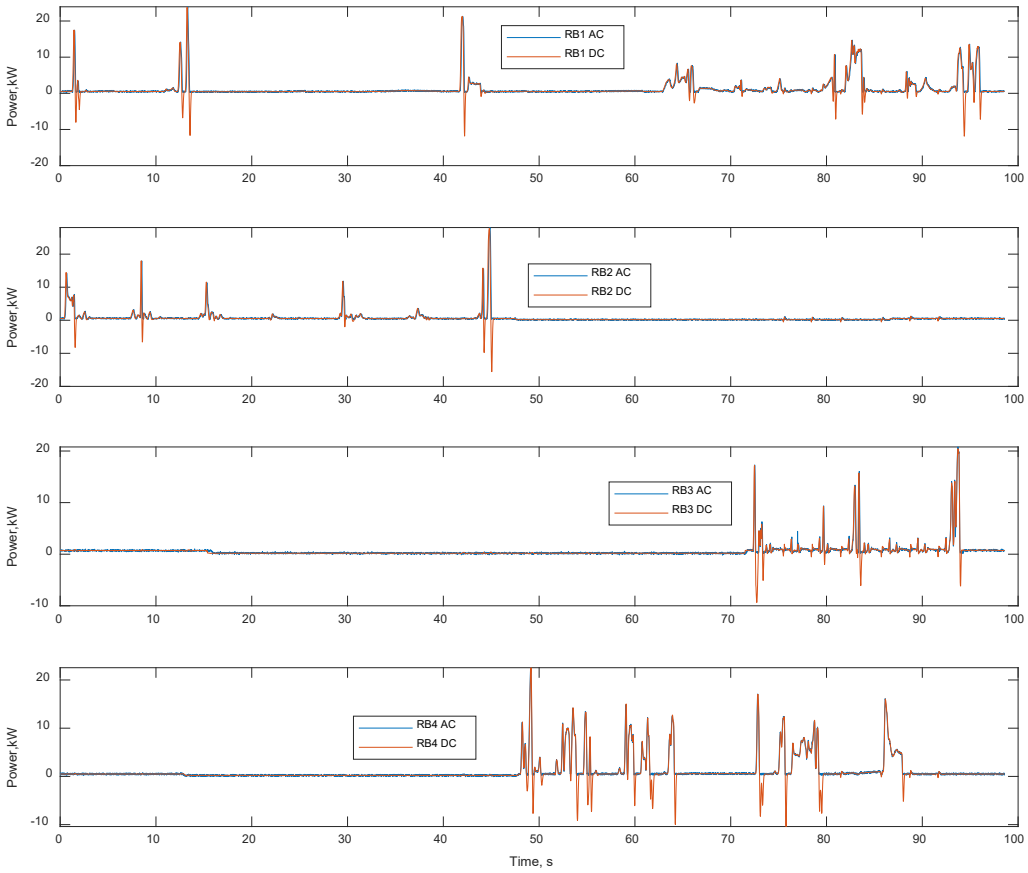

Fig. 4.3. Power flow of a set of four industrial robots for same production cycle, AC and DC based operation.

Calculation of mean power over the production cycle has been done for each industrial robot's control cabinet as well as for combined consumption of all units. The results are summarized in Table 4.1. In all cases, replacing the AC supply-designed control cabinet with a DC-based supply cabinet has reduced average consumed power variation between 5.64 % and 12.55 %. The most significant reduction has been observed of industrial robot picking and placing small metal parts for later processes of joining technologies supported by other industrial robots. All involved industrial robots are equipped with additional tools of weights above 100 kg.

Table 4.1

Result Summary of AC to DC Robot Controller Conversion Test

Robot No.	Related task	Mean power, AC case, kW	Mean power, DC case, kW	Difference (DC case vs AC case), kW	Difference, % of AC case
RB1	Glueing	1.274	1.161	–0.113	–8.87 %
RB2	Riveting	0.693	0.634	–0.059	–8.51 %
RB3	Welding	0.638	0.602	–0.036	–5.64 %
RB4	Part feed	1.211	1.059	–0.152	–12.55 %
Total (4 units)	-	3.818	3.457	–0.361	–9.45 %

Conversion of an AC-based industrial robot application to a DC-based industrial robot application allows utilisation of energy provided by recuperation, and such example of four industrial robots presents a total mean consumed power reduction of 9.45 %. A graphical representation of the total four industrial robot power flow of AC- and DC-based systems is shown in Fig. 4.4.

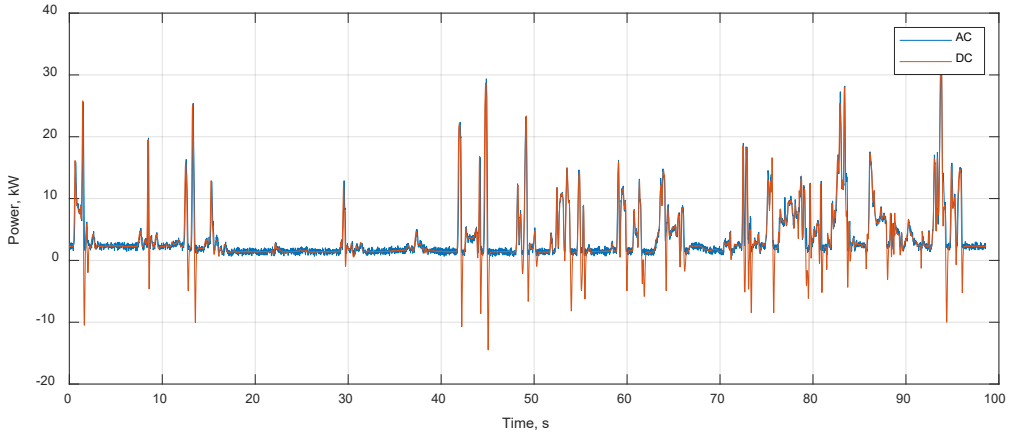

Fig. 4.4. Total power flow of set of four industrial robots, AC and DC based operation.

The performed experimental tests ofreplacing individual market-available AC-designed industrial robot control cabinets with the prototypes for DC-type electrical supply support the hypothesis of energy efficiency improvement related to modification of energy supply system.

Analysis of DC microgrid operation test

The following chapter analyses several aspects of complete DC demostration manufacturing cell operation as a DC microgrid system.

Figure 4.4 represents the obtained power flow results, including thirteen measurement locations within a microgrid. Due to differences in variation and magnitudes of power demand for individual units, the figure shows three groups of devices. All four industrial robot units have similar operational behaviour and are represented in the top axis. Technology tools, li-ion batteries, and PV infeed converter operation have lower power values than 10 kW and are depicted in the middle axis. High power units, being AFE AC/DC converter and spot welding

tool supply are combined in the third axis. The figure represents the operation period in time of 116 seconds, covering one cycle of the continuous process of part assembly involving welding, riveting glueing and related handling of materials. During the test period, power supply from PV panels has also been available and fed into the common DC bus.

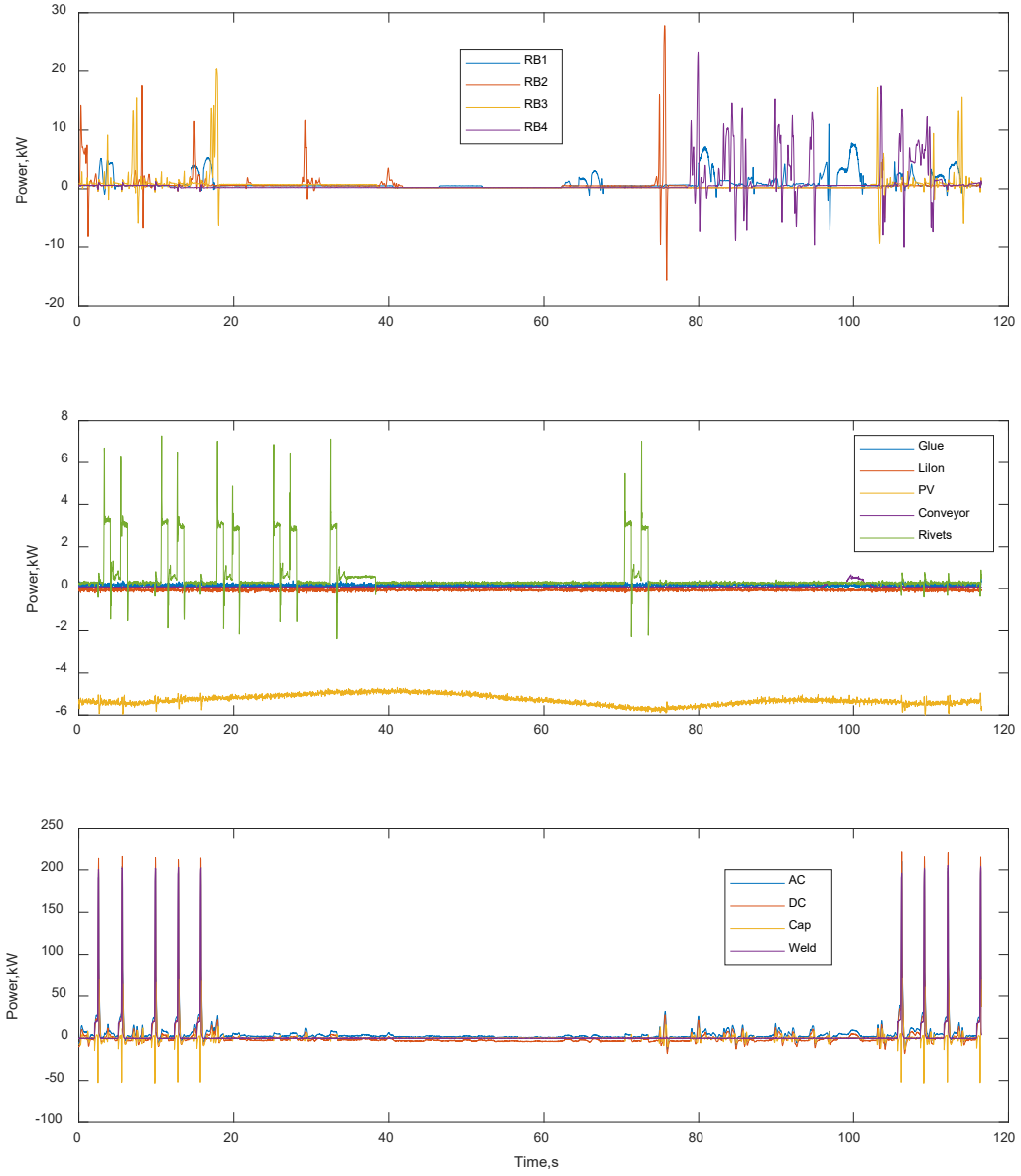

Fig. 4.5. Representation of synchronous power flow measurement results, 13 locations within industrial DC microgrid installation.

Estimation of reused energy potential in industrial application of individual units

One of the particular aspects of interest has been an evaluation of bidirectional energy flow and the relative amount of energy available for reuse due to the advantages of simple energy exchange within DC-type systems in dynamic operation conditions and recuperation events of industrial robots. Eqs. (4.1) and (4.2) represent mean power calculation by separating positive and negative components of power flow P within a certain period of analysis, T.

$$P_{pos} = \frac{\int_0^T P(t)}{T}; P(t) \in [0, \infty) \tag{4.1}$$

$$P_{neg} = \frac{\int_0^T P(t)}{T}; P(t) \in [-\infty, 0) \tag{4.2}$$

Table 4.2 represents the calculation results of bidirectional energy flow for industrial robot units and electrolytic capacitor modules connected to the DC bus of the manufacturing cell.

Table 4.2

Calculation of Mean Positive and Negative Power Flow Values for Individual DC Microgrid Units

DC unit	Related task	P_{pos}, kW	P_{neg}, kW	P_{neg}/P_{pos}, %
RB1	Glueing	1.123	0.044	3.92
RB2	Riveting	0.660	0.040	6.10
RB3	Welding	0.582	0.029	4.95
RB4	Part feed	1.011	0.098	9.71
Total (4 robots)	-	3.376	0.211	6.26
Capacitor bank		1.089	0.677	62.21

The results represent the contribution of industrial robot braking energy reuse cases expressed as negative mean power flow values. The combined operation of four robots led to the average ratio of recuperated power being 6.26 % concerning consumed power. According to motion profiles and manufacturing process needs, individual robot values vary from 3.92 % to 9.71 %. Another DC microgrid element of interest has been a capacitor module installed as an energy buffer element for DC voltage stabilisation. The results represent significant mean power flow values of capacitor operation comparable to single industrial robot units. Accordingly, as the capacitor module has been operated as a dynamic energy storage element, the power flow returned to DC bus has a significantly higher value than industrial robots. The ratio of reused energy with respect to the supplied energy of the capacitor module is 62.21 %. Such results represent the overall efficiency of dynamic operation and related losses of electrolytic capacitors as balancing elements for dynamic operation discussed in the following chapter.

Spot welding power analysis and dynamic effects

Several part-joining manufacturing technologies have been applied within the DC demonstration manufacturing cells. The technology of particular importance has been the aluminium spot welding method performed by a spot welding gun carried by an industrial robot manipulator. The DC-based prototype of the spot welding gun supply and control unit has been

produced by Bosch Rexroth company and designed for operation, replacing the conventional AC welding gun supply unit. The spot welding process presents challenging operation conditions for electrical supply infrastructure due to high power demand of individual spot welding instances of short periods. A complete data set of values at thirteen locations within DC microgrid was obtained through the applied power flow measurement system. The most significant dynamic variation of power flow due to the welding process is represented in the Fig. 4.6. The power flow balance combined of the spot welding tool, both sides of the active frontend AC/DC converter, and the capacitor module power flow are shown.

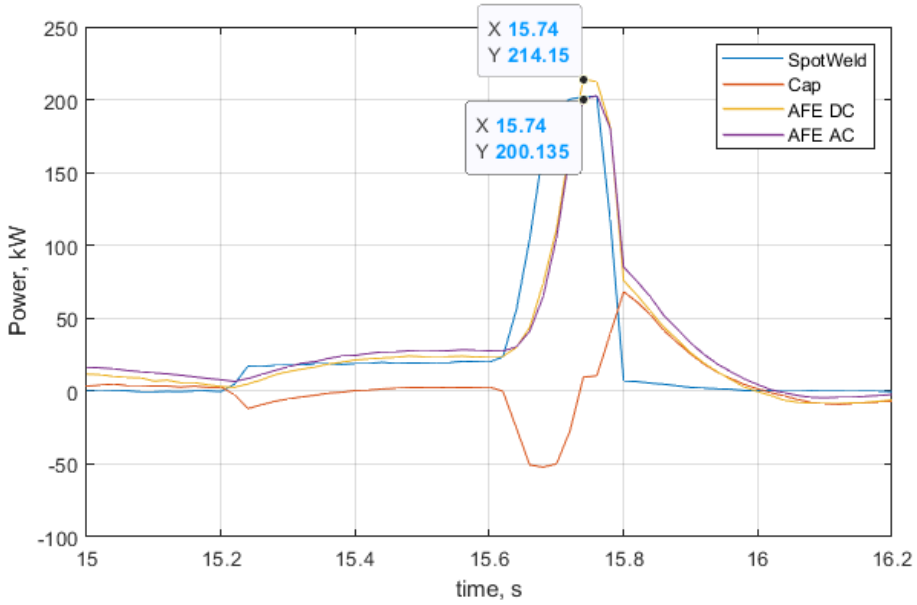

Fig. 4.6. Spot welding instance power of spot welding tool, active front-end AC and DC side and capacitor module.

The single spot welding operation lasts around 0.6 seconds and combines preheating and main welding procedures. The maximum power drawn by the spot welding tool reaches 200 kW. Due to the rapid power demand response of the capacitor module, the power flow is clearly visible. During high power peak rise time the power delivered DC bus capacitor module reaches a 50 kW level. After stabilisation of load power pulse, power supply is provided by the main AC/DC frontend converter. One can observe that the values of the AFE converter DC side exceed those of the AC supply side. The difference can be calculated according to Eq. (4.3), where $P_{AFE\ AC}$ is active fronted AC grid side drawn power and $P_{AFE\ DC}$ is the DC side delivered power flows within a microgrid.

$$P_{AFE\ loss} = P_{AFE\ AC} - P_{AFE\ DC} \tag{4.3}$$

The difference in power flow $P_{AFE\ loss}$ represents the power flow of combined converter power losses including the power used for auxiliary consumption, such as 24 V automation and safety equipment power supply, SCADA system and power commutation equipment control.

Therefore, a more detailed analysis of AFE converter loss power flow combined welding process is presented in Fig. 4.7.

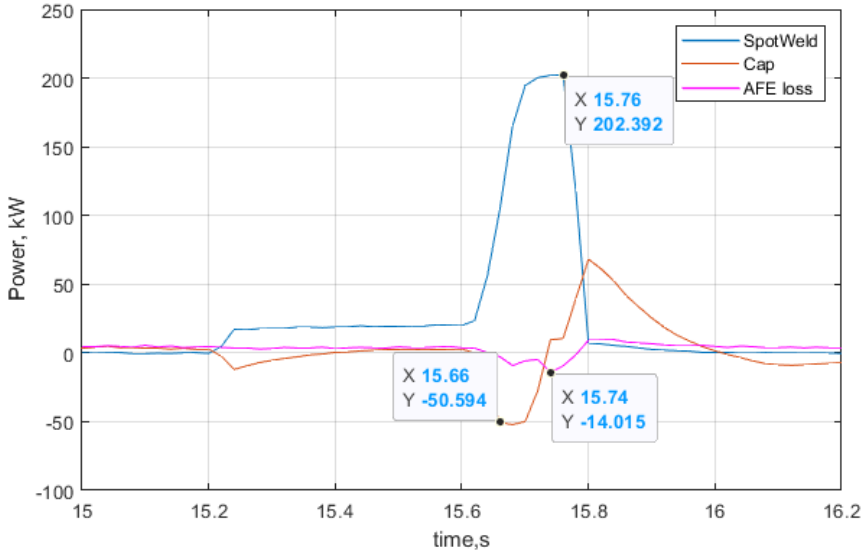

Fig. 4.7. Example of power flow drawn from the capacitor module and reverse pover flow of AC/DC converter internal circuits.

The dynamics of power consumption represent the behaviour that requires power for spot welding tools, which has also been provided from internal devices and circuits within the AC/DC converter cabinet. The AC/DC converter has internal filter capacitors that behave similarly to the main capacitor module and provide power as the main capacitor module power is reduced.

The AFE internal loss power variation with respect to AFE DC side power demand is mapped as shown in Fig. 4.8.

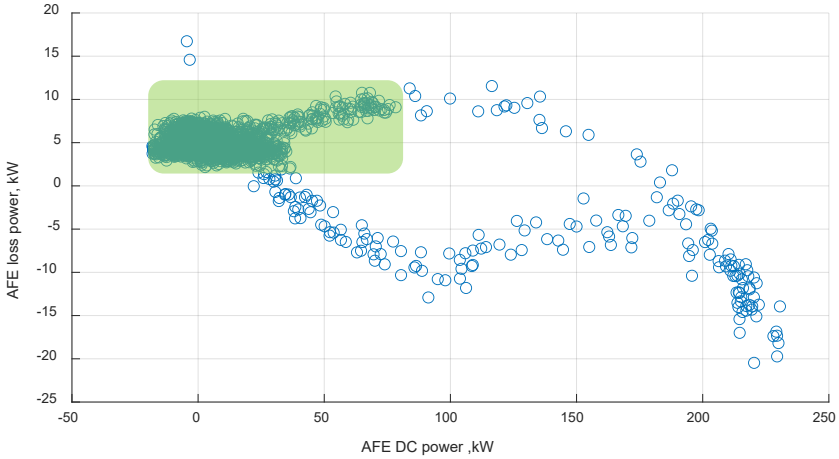

Fig. 4.8 Active front-end converter internal loss power flow vs active front-end converter supplied DC power.

After observing the operating point density in time over the whole manufacturing process, it is visible that internal AC/DC converter loss and auxiliary equipment power demand are aggregated at 0 kW to 10 kW level during stable operation below 75 kW. The sparse operating points outside the green area represent pulsed power effects related to spot welding power demand.

DC side power flow balance evaluation using superposition approach

In order to verify the dynamic performance of the applied multipoint synchronous power flow measurement system and measurement result data, the calculation of power flow balance of 12 location power flows has been done. Adding all 12 power flows connected to DC bus would provide zero sum in idealized case if physical electrical losses were neglected and no measurement error would be present. According to such a superposition approach, the value *SumDC* has been introduced. The results obtained over the time frame are presented in Table 4.3.

Table 4.3

Key Results of DC Bus Power Flow Balance Value *SumDC* Calculation

	Max. value, kW	**Min. value, kW**	**Mean value, kW**
SumDC	44.29	–27.64	0.180

Analysis of the obtained *SumDC* parameter with respect to DC system operation dynamics reveals that increased deviation of DC bus power flow balance calculation has been obtained during peak power demand instances. Figure 4.9 represents the observed balance deviation with respect to welding power peak demand.

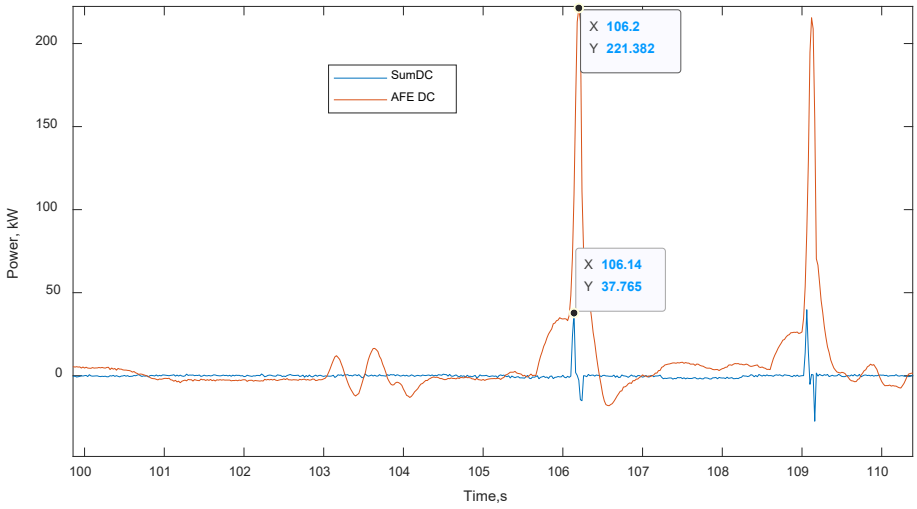

Fig. 4.9. DC bus power flow balance parameter *SumDC* variation during spot welding process compared to AC/DC AFE converter supplied DC power.

The mean value of *SumDC* power flow value over the full time period of DC microgrid observation reaches the value of 180 W. The dynamic variation during steep power flow rate of rise or fall can be explained by potential errors of measurement that could be induced by the dynamic behaviour of applied current measurement equipment based on the Hall effect current clamps.

Power balance of DC manufacturing cell

In order to obtain an overview of mean power flows over continuous manufacturing process and related energy distribution within microgrid system, Fig. 4.10 has been developed.

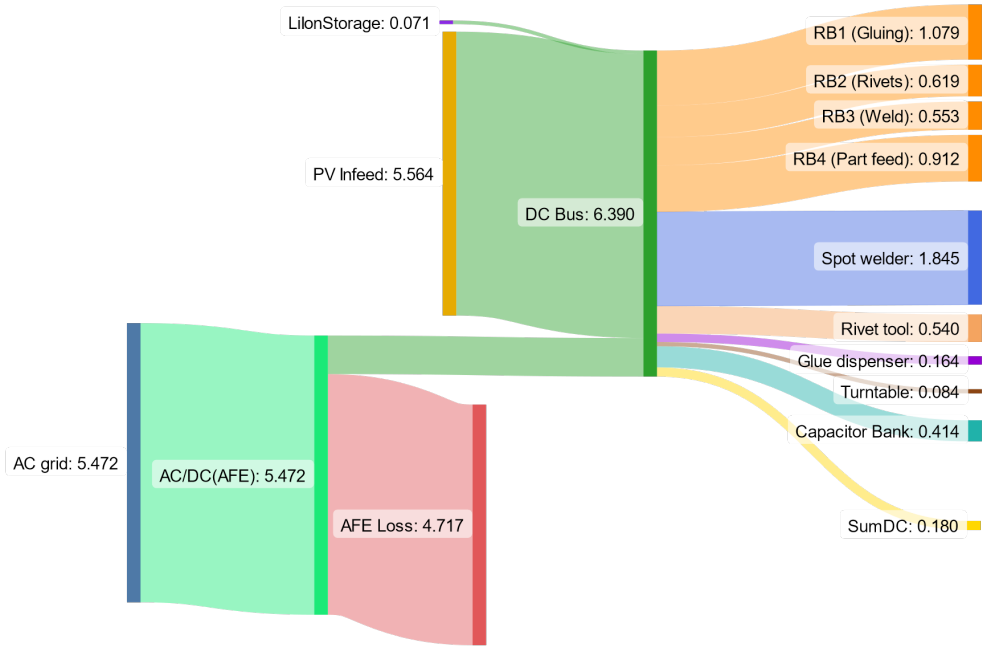

Fig. 4.10. Full DC manufacturing cell mean power distribution based on synchronous 13-point power flow measurement system test data.

- Power sources

The particular configuration of DC microgrid has two major power supply sources, being AC grid and PV panels (PV infeed) of average renewable power flow of 5.64 kW. The connected li-ionbattery module has operated in standby mode with a neglegable contribution.

- Central AC/DC active front-end (AFE) operation

The main AC/DC bidirectional converter operation has been analysed by calculating the internal power demand $P_{AFE\ loss}$ over the operational period. The average value of 4.72 kW may appear large compared to technology-related loads discussed further and within the same scale as solar renewable power delivered. However, this power flow represents several functional needs of the whole DC installation, i.e., 24 V supply of automation and safety equipment and several control and operator panels, electrical cabinet air conditioning and converter losses being the most significant. Considering the ability of selected infeed converter configuration for large industrial DC microgrid system power supply, such auxiliary power demand can also be considered reasonable.

- Industrial robot and technology tool consumption

The group of four industrial robots has similar mean load power values in the range of around 0.5 kW to 1 kW. As discussed before, the power drawn from the DC bus has been reduced by recuperation energy utilization. The most significant technology load has been the spot welding application, reaching around 1.8 kW mean load power, but the requirements imposed for DC

microgrid operation due to high peak power are fundamental for design of electrical installation. Other technology loads have low average power consumption requirements of 0.6 kW or less.

- Capacitor module operation and total balance of DC bus power

Due to dynamic power flow behaviour, the overall performance of the electrolytic capacitor module installed on the DC bus represents a mean power requirement of 0.414 kW. Such value has been obtained according to dynamic operation of around 50 kW discharge and 60 kW charging peak power pulses related to common DC system balancing needs imposed by spot welding application. An average power of 0.414 kW represents combined mean losses due to electrolytic capacitor series resistance character and related conduction losses of modular arrangement of individual cells.

The value of *SumDC* parameter 0.18 kW represents a combination of all DC side power flow measurement equipment errors mainly related to dynamic current detection during steep power change instants. The other component contributing to the overall result of *SumDC* loss power is introduced by the real physical connection of individual devices to the DC busbar system, therefore, physical losses are also included. The extensive cross section of selected copper busbars installed with respect to the average combined DC bus load power being 6.39 kW allows concluding that total expected conduction losses are also within the range of estimated *SumDC* power flow calculation.

Installation of a laboratory scale robotic manufacturing DC

The verification of DC microgrid-based operation for small-scale production tasks involving a few industrial robots has been done by means of a DC microgrid laboratory setup assembled in a single room at the RTU faculty building, as represented before. The author's Publications 6 and 7 are related to this aspect.

Analysis of individual robot energy reuse potential has been done within various scenarios, from a single unit to a combination of three robots. The physical implementation has been achieved by using a DC supply converted KUKA Quantec series 210 kg payload industrial robot prototype and two DC power flow emulators composed of coupled induction electrical machines and respective variable frequency drives with a common control unit. The interface active front-end (AFE) AC/DC converter of 65 kW nominal power has been used as the main power supply. Table 4.4 represents the summary of test configurations performed for DC microgrid analysis. Test scenarios 1 to 3 present an analysis of single robot and emulators performing the tasks based on industrial power consumption obtained in the industrial application at the factory. Tests 4 and 5 are performed as simultaneous operations of several industrial robots within the same production area.

Table 4.4

Test Configurations for DC Microgrid of Industrial Robot Applications

Configuration	DC KUKA robot (Prob)	Drive emulator EM1	Drive emulator EM1
Test 1	Welding		
Test 2		Part feed	
Test 3			Rivet punching
Test 4		Part feed	Rivet punching
Test 5	Welding	Part feed	Rivet punching

Figure 4.11 represents original power demand profiles used for interconnected DC microgrid analysis for small enterprise applications performed in RTU DC laboratory microgrid installation.

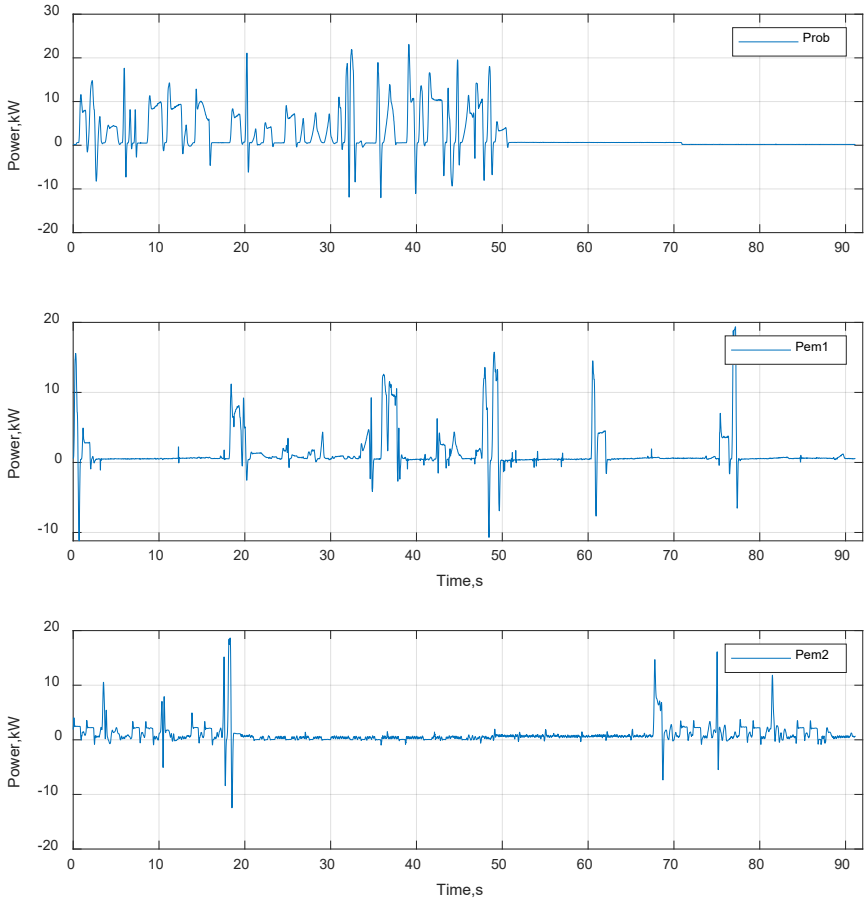

Fig. 4.11. The set of individual industrial robot consumption power profiles: KUKA DC robot *Prob*, and two drive emulators *Pem1* and *Pem2*.

As the complexity of a system is increased, a total combination of three DC microgrid load units representing industrial robots is achieved. A total combination of central AC/DC converter power flow and DC microgrid load profiles is presented in Fig. 4.12.

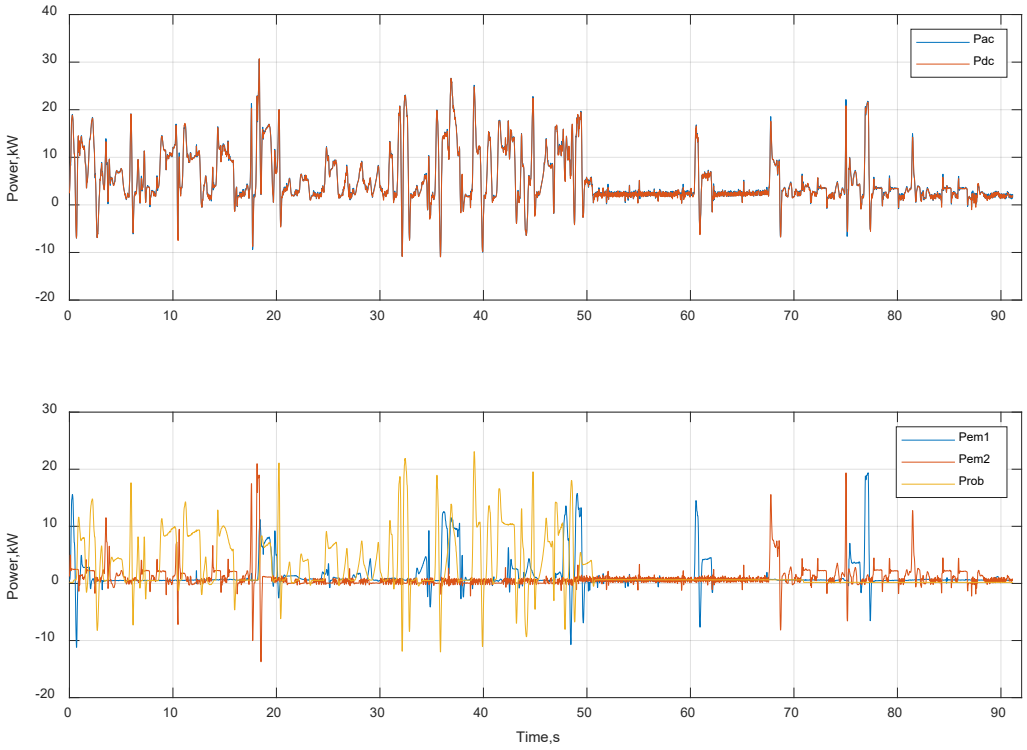

Fig. 4.12. Dynamic power flow of Test5 configuration with respective AC grid (*Pac*) and DC microgrid infeed power (*Pdc*) flows (top axis) and all three industrial robot loads (*Prob, Pem1, Pem2*) combination (bottom axis).

The obtained power flows are analysed by calculating the mean load and recuperated power flow values. Figure 4.13 represents an overview of power flow direction analysis by mean power flow extraction within the manufacturing task time period. *Pafe.AC* and *Pafe.DC* are active front-end AC/DC converter measurements on the AC and DC sides. *Prob, Pem1,* and *Pem2* are individual DC load equipment power flows. As total power consumption needs are increased by expanding the DC microgrid load group, active front-end converter power flows are increased for load and recuperation operation over the manufacturing cycle.

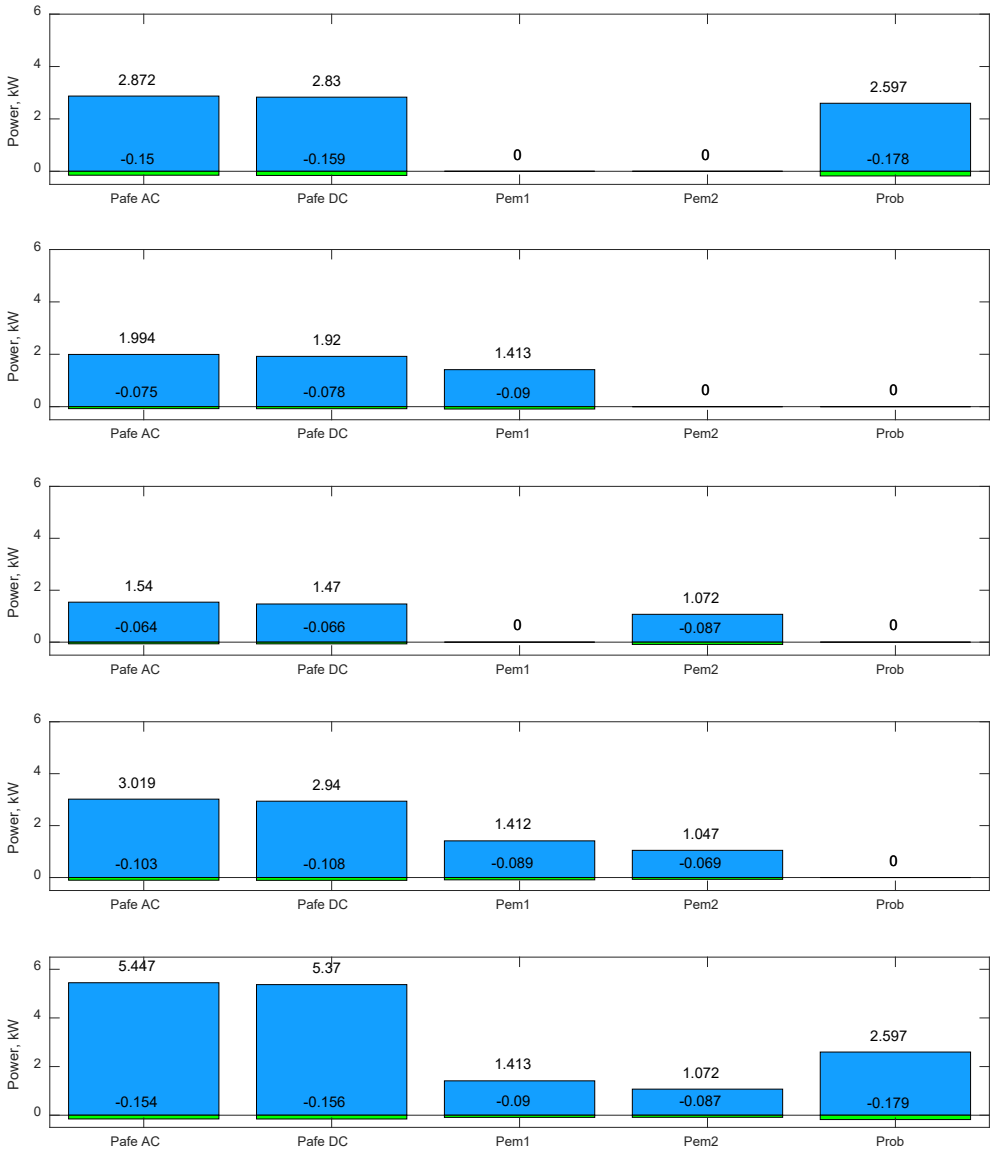

Fig. 4.13. Summary results of five DC microgrid configurations: Test1 (top axis) to Test5 (bottom axis). Mean load power (positive values) and recuperated power (negative values) flow estimation based on experimental measurement results within the 91.14-second manufacturing task.

Figure 4.14 has a similar structure as the previous analysis representation. However, the proportional ratio expressed in % of returned power flow with respect to direct load power flows is visualized. According to Fig. 4.14, it has been observed that the total recuperated energy component is reduced by an expansion of the DC side load unit number with bidirectional power flow capacity. The excess energy generated within the DC bus by robot

braking results in the negative power flow of the front-end converter DC side *Pafe.DC*. In the case of single-unit operations, the interconnected configurations of several robot units represent a reduction of total recuperated power to 2.9 % from 4.07–5.07 %. It can be observed that the energy potential for reuse with the robot (*Prob*) or emulators (*Pem1* and *Pem2*) is higher than that obtained on the AC power grid side or intermediate DC link. It is due to internal consumption being drawn from the DC link for control logic supply at a 24-Volt level as well as losses of bidirectional AC/DC converter feeding energy back into the AC grid.

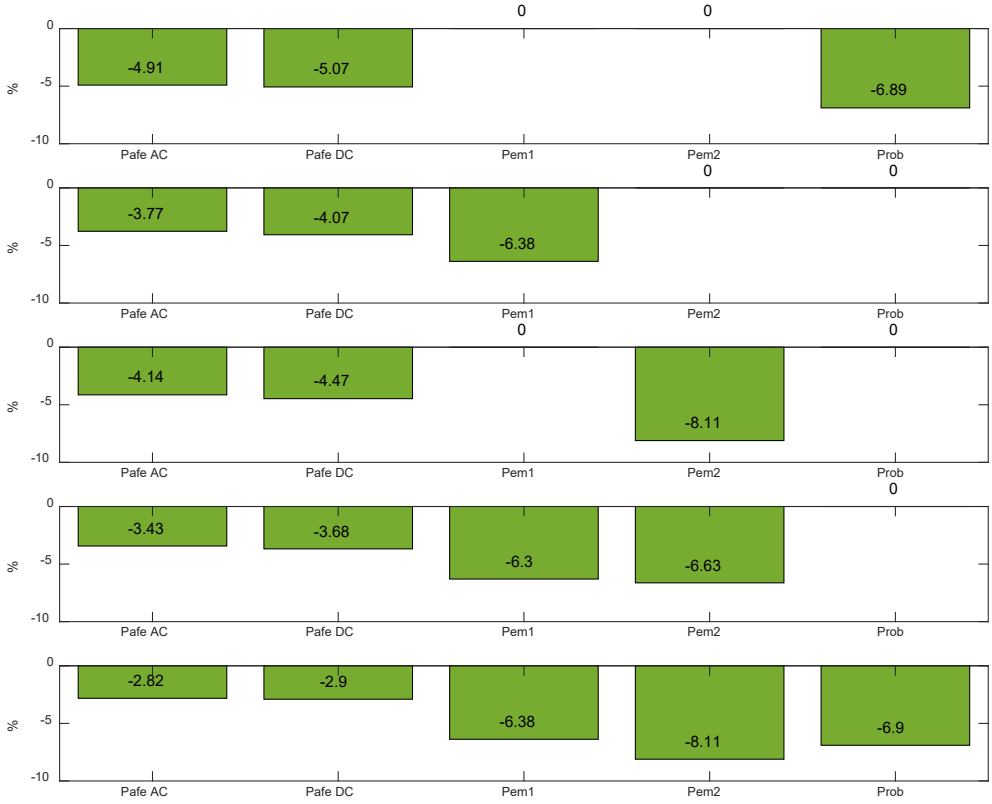

Fig. 4.14. Summary results of five DC microgrid configurations: Test1 (top axis) to Test5 (bottom axis). The obtained ratio in % represents the recuperated power flow compared to the consumed load power flow over the 91.14-second cycle of measured power flows.

Table 4.5 represents an overview of the mean power flow values obtained within the aforementioned experimental test configurations Test1 to Test5. Total power distribution analysis within microgrid installation allows estimation of average power losses within intermediate AC/DC power conversion and DC side distribution processes. Power loss related to active frontend AC/DC conversion losses and converter auxiliary loads is calculated according to Eq. (4.4), where *Pafe.AC* and *Pafe.DC* are converter AC and DC side power flow values.

$$Ploss.afe = Pafe.AC - Pafe.DC \quad (4.4)$$

Power loss *Ploss.DCbus* related to DC electrical connections realized by 16 mm^2 cables and additional 24 V power supply units can be calculated according to Eq. (4.5), where *Pafe.DC* is the power supplied on the DC output of AC/DC converter and *Prob*, *Pem1*, *Pem2* are input connections of robot and drive emulator units.

$$Ploss.DCbus = Pafe.DC - Prob - Pem1 - Pem2 \quad (4.5)$$

Total losses, *Ploss.total*, that are present and not directly related to the operation of individual DC microgrid connected manufacturing tools can be estimated by calculation according to Eq. (4.6).

$$Ploss.total = Ploss.DCbus + Ploss.afe \quad (4.6)$$

Table 4.5

Summary of Average Power Flow and Power Loss of Five Test Cases

		Experimental setup				
Units	**Quantity**	**Test1**	**Test2**	**Test3**	**Test4**	**Test5**
kW	*Pafe.AC*	2.98	1.919	1.476	2.915	5.293
	Pafe.DC	2.90	1.837	1.402	2.83	5.213
	Prob	2.418				2.417
	Pem1		1.323		1.323	1.323
	Pem2			0.985	0.977	0.981
	Ploss.afe	0.080	0.082	0.074	0.085	0.080
	Ploss.DCbus	0.486	0.514	0.417	0.530	0.492
	Ploss.total	0.566	0.596	0.491	0.615	0.572
Relative loss analysis vs *Pafe.AC*						
%	*Ploss.afe*	2.68	4.27	5.01	2.92	1.51
	Ploss.DCbus	16.28	26.78	28.25	18.18	9.29
	Ploss.total	18.96	31.06	33.27	21.10	10.81

The observation of summary results supports the hypothesis of increased energy efficiency by the implementation of an interconnected DC microgrid system for industrial robot-type loads. The AC/DC converter loss level represents a stable average power value of around 80 W. The component of overall DC microgrid loss power is reduced as a number of connected load units expands the system. The setup of two interconnected load units represents a 21.1 % power loss, and the value has reduced to 10.81 % by increasing the number of three interconnected load units.

Influence of industrial robot tool mass on braking energy potential

In order to observe the influence of production tool mass on electrical energy potential available for reuse, experiments with varying load have been done based on the same robot motion trajectory program execution (Publication 6). The specific industrial tool replica (Fig. 4.15) has

been applied with steel plates, allowing incremental changes of total mass at the end of the robot.

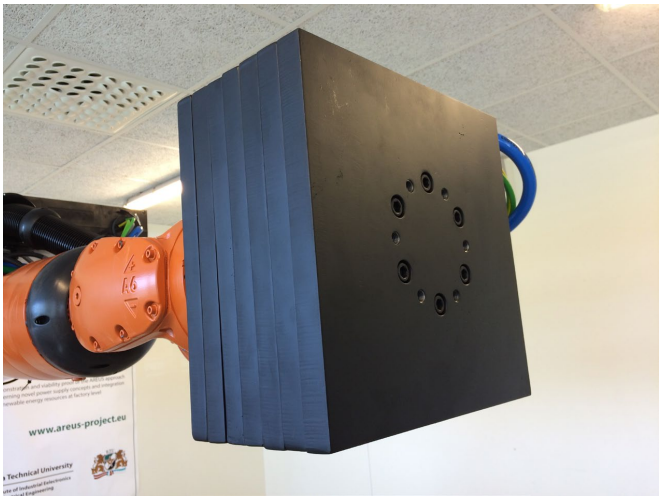

Fig. 4.15. Test tool replica for various tool mass experiments.

Bidirectional power flow measurements have been obtained for the same motion trajectory execution in various tool mass cases, as represented in Fig. 4.16.

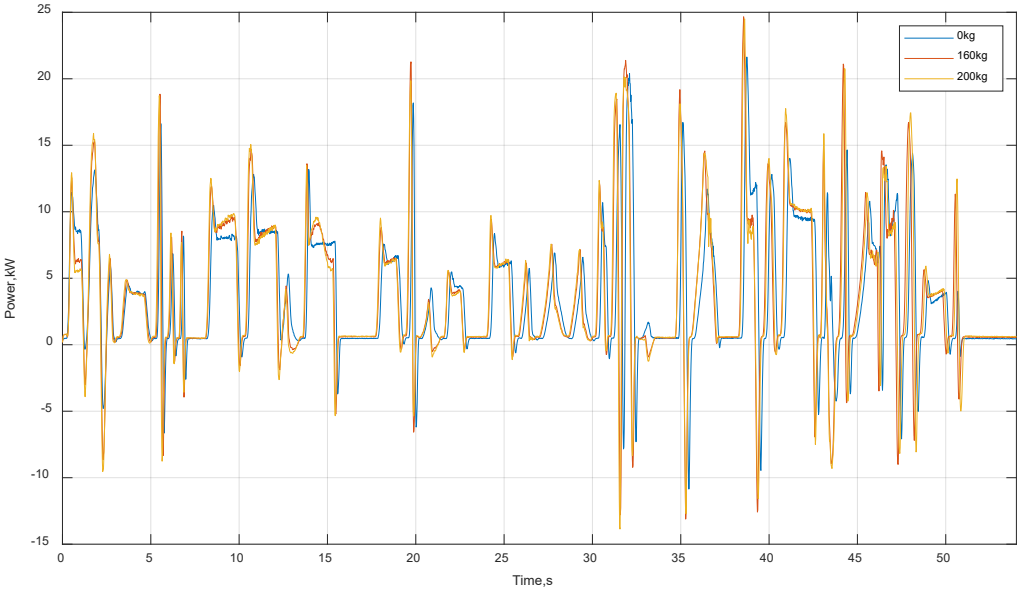

Fig. 4.16. Power flow profiles at various tool mass (0 kg, 160 kg, 200 kg).

Numerical evaluation results support the assumption that the application of braking energy reuse is more relevant for large production tools with significant total mass.

Table 4.6

Average, Consumed and Recuperated Power Flow by Tool Mass Variation

Tool mass, kg	Average total power, kW	Average consumed, kW	Average recuperated, kW	Recuperated vs consumed, %
0	3.612	3.821	0.208	5.45
159.3	3.688	4.031	0.343	8.52
201.3	3.676	4.055	0.378	9.34

According to the observed correlation between the tool mass and energy reuse, potential suitable applications for DC-related electrical system modification or replacement can also be selected. The Thesis has provided an insight into industrial robot applications related to automotive manufacturing processes; however, it can be expanded to other industrial sectors, providing similar parameters of industrial robot tool mass and motion characteristics.

CONCLUSIONS

The initial hypotheses of DC-based energy exchange and supply system relevance for industrial applications involving several industrial robot units and related manufacturing equipment have led to gradual introducing of DC-based electrical systems, starting from standard AC supply industrial robots to industrial DC microgrid installation.

Modification of typical AC supply-based industrial robots by DC shared bus configuration leads to a reduction of average power for the same motion operation and task for more than 20 %, depending on the applied tool payload and dynamics of the motion program.
A new power electronics-based module circuit for power flow control has been successfully developed and patented. An equivalent electrical system model has been developed for further optimization and modular electrical device design, leading to industrial prototypes of a shared DC bus industrial robot system.
A single DC power infeed microgrid demonstration setup of multiple robot systems has been physically implemented on a laboratory scale, and respective experimental measurements and a model of AC/DC infeed converter have been developed.
The operation of a small-scale industrial DC microgrid involving up to three industrial robots demonstrates the potential of reused energy up to 15 %, which is verified by physical experiments in the university laboratory and market available AC/DC conversion equipment. The design for the experiment has enabled new test setups for future emulation experiments and dynamic testing of DC industrial equipment.
Experimental tests of direct AC to DC industrial robot controller architecture substitution for a group of four units and the same manufacturing task reveal a reduction of average power consumption by 9.5 %.
A real-time synchronized data set was experimentally obtained in a large-scale factory-level DC microgrid setup. Detailed analysis of dynamic power flow between individual electrical units and estimation of reused energy has revealed up to 6.5 % energy reuse potential of DC-type industrial robot application of four units.
Overall loss calculation and distribution within the system based on 13 location synchronized power flow measurements have been analysed, and respective future optimization directions have been defined.

Results and experiments support the proposed DC-based electrical system applicability hypothesis for energy efficiency improvement of industrial robot-related industrial manufacturing applications.
Knowledge obtained during the development highlights the importance of further research on DC-type industrial electrical system development methodologies and new design tools supported by experimentally verified models for optimal dimensioning and component selection in real installations, thus enabling new flexible DC microgrid installations for better utilization of advantages expected in future dynamic energy systems.

REFERENCES

[1] IFR – international Federation of Robotics, "World robotics – Industrial Robotics 2023."

[2] IFR International federation of Robotics, "European Union: Industries Invest Heavily in Robotics – International Federation of Robotics." [Online]. Available: https://ifr.org/ifr-press-releases/news/eu-industries-invest-heavily-in-robotics. [Accessed: 28-Sep-2023].

[3] "A European Green Deal." [Online]. Available: https://commission.europa.eu/strategy-and-policy/priorities-2019-2024/european-green-deal_en. [Accessed: 29-Sep-2023].

[4] "The Green Deal Industrial Plan." [Online]. Available: https://commission.europa.eu/strategy-and-policy/priorities-2019-2024/european-green-deal/green-deal-industrial-plan_en. [Accessed: 29-Sep-2023].

[5] R. W. De Doncker, "Power electronic technologies for flexible DC distribution grids," *2014 Int. Power Electron. Conf. IPEC–Hiroshima – ECCE Asia 2014*, pp. 736–743, 2014.

[6] "REPowerEU: affordable, secure and sustainable energy for Europe." [Online]. Available: https://commission.europa.eu/strategy-and-policy/priorities-2019-2024/european-green-deal/repowereu-affordable-secure-and-sustainable-energy-europe_en. [Accessed: 29-Sep-2023].

[7] "Automation and Robotics for EUropean Sustainabile manufacturing | AREUS | Project | Fact sheet | FP7 | CORDIS | European Commission." [Online]. Available: https://cordis.europa.eu/project/id/609391. [Accessed: 29-Sep-2023].

[8] "dc-industrie.zvei.org/en - dc-industrie.zvei.org - Microsite." [Online]. Available: https://dc-industrie.zvei.org/en/. [Accessed: 25-Sep-2023].

[9] "USB-type C to become EU's common charger by end of 2024 | News | European Parliament." [Online]. Available: https://www.europarl.europa.eu/news/en/headlines/society/20220413STO27211/usb-type-c-to-become-eu-s-common-charger-by-end-of-2024. [Accessed: 29-Sep-2023].

[10] "CurrentOS Foundation." [Online]. Available: https://currentos.foundation/. [Accessed: 25-Sep-2023].

[11] "The Second Grid – DC Systems." [Online]. Available: https://www.dc.systems/vision/the-second-grid. [Accessed: 25-Sep-2023].

[12] "Flexible Electrical Networks | Research Campus FEN Aachen." [Online]. Available: https://www.fenaachen.net/. [Accessed: 29-Nov-2021].

[13] "NExT Factory-Efficient Smart Green / Schaltbau." [Online]. Available: https://www.schaltbau.com/en/about-us/portrait/next-factory-efficient-smart-green/. [Accessed: 25-Sep-2023].

[14] "'Factory 56': Mercedes-Benz Cars significantly increases flexibility and efficiency with 'Factory 56'| Mercedes-Benz Group > Innovation > Digitalisation > Industry 4.0." [Online]. Available: https://group.mercedes-benz.com/innovation/production/factory-56.html. [Accessed: 25-Sep-2023].

[15] "National energy and climate plans." [Online]. Available: https://commission.europa.eu/energy-climate-change-environment/implementation-eu-countries/energy-and-climate-governance-and-reporting/national-energy-and-climate-plans_en. [Accessed: 29-Sep-2023].

[16] IFR – international Federation of Robotics, "WR 2021 Industrial Robots – Sources & Methods," 2021.

[17] R. Murray, Z. Li, and S. Sastry, *A mathematical introduction to robotic manipulation*, vol. 29. 1994.

[18] Paryanto, M. Brossog, J. Kohl, J. Merhof, S. Spreng, and J. Franke, “Energy Consumption and Dynamic Behavior Analysis of a Six-axis Industrial Robot in an Assembly System,” *Procedia CIRP*, vol. 23, no. C, pp. 131–136, Jan. 2014.
[19] D. Meike, “Multi-Domain Model for the Evaluation of Large Scale Robotic Applications within Production,” *Riga Tech. Univ. 53rd Int. Sci. Conf. Dedic. to 150th Anniv. 1st Congr. World Eng. Riga Polytech. Inst. / RTU Alumni Dig.*, pp. 113–113, 2012.
[20] A. Rassõlkin, H. Hõimoja, and R. Teemets, “Energy saving possibilities in the industrial robot IRB 1600 control,” in *2011 7th International Conference-Workshop Compatibility and Power Electronics, CPE 2011 – Conference Proceedings*, 2011, pp. 226–229.
[21] D. Meike, “Increasing Energy Efficiency of Robotized Production Systems in Automobile Manufacturing,” 2013.
[22] D. Meike and L. Ribickis, “Recuperated energy savings potential and approaches in industrial robotics,” in *IEEE International Conference on Automation Science and Engineering*, 2011, pp. 299–303.
[23] O. Bormanis, “Increasing Reliability of Robotized Manufacturing Systems,” RTU, Riga, 2022.
[24] C. M. Hackl, A. G. Hofmann, R. W. De Doncker, and R. M. Kennel, “Funnel Control for Speed & Position Control of Electrical Drives: A Survey.”
[25] “Gleichstrom im Niederspannungs-bereich Deutsche Normungs-Roadmap Version 2 VDE | DKE Roadmap.”
[26] ZVEI & consortium DC-INDUSTRIE2, “DC-INDUSTRY_Systemconcept-V2,” DC-INDUSTRIE & ZVEI, 2022.
[27] P. Apse-Apsitis, A. Avotins, and L. Ribickis, “A different approach to electrical energy consumption monitoring,” In: *2014 16th European Conference on Power Electronics and Applications*, 2014, pp. 1–5.
[28] R. Rodrigues, Y. Du, A. Antoniazzi, and P. Cairoli, “A Review of Solid-State Circuit Breakers,” *IEEE Trans. Power Electron.*, vol. 36, no. 1, pp. 364–377, Jan. 2021.

Armands Šenfelds was born in 1986 in Riga. He received a Bachelor's degree in 2009 and a Master's degree in 2010 in Electrical Engineering from Riga Technical University (RTU), Latvia. In 2012, he received a Master's degree in Electrical Power Engineering from RWTH Aachen University, Germany. Since 2013, he has been a research assistant, researcher and lecturer at the Institute of Industrial Electronics and Electrical Engineering (IEEI) of Riga Technical University.

He has been a member of the IEEE association since 2008 and has served in various positions in the IEEE Latvian Section. He has been a Board member of the German Academic Exchange Service Alumni Club Latvia since 2013.

His research interests are related to power electronics for electrical drives, robotics, DC electrical systems, and efficient electrical energy utilization applications.